ChemComm

FEATURE ARTICLE

View Article Online
View Journal | View Issue

Cite this: *Chem. Commun.*, 2024, **60**, 14717

Ionic liquid-assisted sustainable preparation of photo-catalytically active nanomaterials and their composites with 2D materials†

Kanica Sharma and Tejwant Singh Kang *‡

The preparation of nanomaterials employing ionic liquids (ILs) and surface active ionic liquids (SAILs) in a relatively sustainable manner for different applications is reviewed. ILs offer structure directing and templating effects *via* inherent bi-continuous structures formed by the segregation of polar and non-polar domains. On the other hand, SAILs offer a structure-directing effect governed by their ability to lower the surface tension, self-assembling nature and interaction with precursors *via* ionic head groups. Binary mixtures of ILs with other relatively greener solvents or utilization of metal-based ILs (MILs), which act as precursors of metal ions, templates and stabilizing agents propose a new way to prepare a variety of nanomaterials. The introduction of SAILs that exfoliate 2D materials under low-energy bath sonication and also aid in photoreduction and stabilization of photocatalytically active nanomaterials at the surface of 2D materials poses a distinctive perspective in sustainable preparation and utilization of nanomaterials in different photocatalytic applications. The present feature article reviews the employment of distinctive properties of ILs in precise morphological control of nanomaterials, and their after-effects on their catalytic efficiencies.

Received 26th September 2024,
Accepted 14th November 2024

DOI: 10.1039/d4cc05001k

rsc.li/chemcomm

"*Nanotechnology*" is a term related to the synthesis and investigation of materials having ultrafine dimensions in the range of 1–100 nm.[1,2] The materials in this size range exhibit unique properties due to an enhanced surface-to-volume ratio, quantum confinement, and other effects, not available in bulk scale.[3] There is a plethora of nanoparticles (NPs) comprising a variety of materials ranging from metals,[4] semiconductors,[5] quantum dots (QDs),[6] and their combinations,[7] varying in dimensions and properties useful in various applications.[8–12] The advent of graphene[13] and various other two-dimensional (2D) materials[14–20] has further revolutionized the field. The conjunction of 2D materials with nano-architectures resulted in better characteristic properties not exhibited by individual components[21–24] owing to heterojunction formation. The synthetic route followed for the preparation of nanomaterials influences the properties of nanomaterials[25] where the conventional synthetic methods generally employ volatile organic solvents (VOSs), stabilizers or templating agents (surfactants and polymers, *etc.*), strong reducing agents along with high-intensity energy sources and other costly instruments for precise shape and size control of the NPs.[26–29] These approaches are very proficient in providing distinctive NPs; however, their utilization is limited by economic and environmental liabilities. However, the use of organic polymers as economical alternatives to conventional stabilizers contributed to the field of nanotechnology.[30] Polymers, such as polyvinylpyrrolidone (PVP)[31] and polystyrene,[32,33] act as templating agents, owing to various electrostatic interactions among their functionalized monomeric units and the metal ions for efficient adsorption at the NP surfaces. The stabilizing and reducing abilities of polymers in an aqueous medium make them highly desired agents for size and shape control during the preparation of NPs.[34]

Similarly, different approaches are utilized to prepare or exfoliate 2D materials. For example, the preparation of graphene derivatives (graphene oxide and reduced graphene oxide) is generally achieved by Hummers' process, which involves H_2O_2, HNO_3, H_2SO_4, and $KMnO_4$, with the process taking hours to complete (more than 5–6 steps).[35] Other methods involve the use of conventional ionic surfactants and organic solvents for liquid phase exfoliation of 2D materials.[36] Surfactants lower the interfacial tension and intercalate between the layers of the 2D materials dispersed in water, a requisite for exfoliation.[16,37] However, the point charge at the ionic head group in conventional surfactants reduces their efficacy in exfoliating 2D materials whereas most of the organic solvents are toxic.

The use of chemicals is bound to chemistry, however, as humans and prominent receivers in biological ecosystems, it is

Department of Chemistry, UGC Centre for Advanced Studies (CAS-II), Guru Nanak dev University, Amritsar-143005, India. E-mail: tejwantsinghkang@gmail.com

† This feature article is dedicated to Prof. Nobuo Kimizuka, Professor, Department of Applied Sciences, Graduate School of Engineering, Kyushu University, Japan on his 65th Birthday, who was among the pioneers in preparing IL templated hollow TiO_2 and discrete gold nano-architectures.

‡ Current Address: Department of Applied Chemistry, Graduate School of Engineering, Kyushu University, 744 Moto-oka, Nishi-ku, Fukuoka 819-0395, Japan.

our responsibility to adopt environment-friendly yet efficient strategies for experimental design based on the "*12 principles of Green Chemistry*".[38,39] The combination of nanotechnology and sustainability appears promising and is expected to provide the scientific community with novel discoveries and useful applications while least affecting the environment. Many approaches have been reported in recent times employing less harmful reagents in terms of their impact on the environment and providing distinctively featured nanomaterials.[40–43] In this regard, the usage of plants or other biological extracts[44] has been employed to prepare a variety of noble metal NPs,[45] semiconductor nanocrystals,[46] and quantum dots.[47] The chemical entities in plant extracts act as templating and reducing agents while exerting marginal control over the size and structural features owing to their inability to control the rate of nucleation and growth of the NPs. Many times, varying compositions of the extracts result in inconsistency in the properties of NPs and hence reproducibility is a major concern.

During the past 2 decades, ionic liquids (ILs)[48] have attracted great interest from researchers as a new class of benign solvents for diverse applications,[49–55] alternative to VOSs. ILs were employed as suitable media for the preparation of nanoparticles (NPs)[56–63] stabilized by the inherent bi-continuous structures of ILs.[64–67] The tailoring of alkyl chains of ILs offered an opportunity to prepare a new class of surfactants called surface active ionic liquids (SAILs). SAILs lower the surface tension of water and other solvents and undergo self-assembly in a diverse array of solvents akin to conventional ionic surfactants.[68–70] SAILs many a time show better surface activity owing to large-sized ionic head groups with delocalized charge and functionalized alkyl chains.[71–73] SAILs exert electrostatic, hydrophobic, and non-covalent interactions, which play an important role in controlling the surface activities and hence, the aggregation of SAILs, which are not possessed by conventional ionic surfactants with point charges. For example, imidazolium-based SAILs have charge delocalization in the imidazolium head group which renders it less polarized and results in decreased electrostatic repulsions among the head groups and facilitates aggregation at relatively lower critical micelle concentration (cmc) as compared to conventional ionic surfactants.[74] Non-covalent interactions (hydrogen bonding, π–π stacking) are considered to be responsible for compact packing of aromatic head groups in micellar aggregates.[75] Hence, all these structural features of SAILs account for their enhanced surface activity and result in the formation of stable aggregates not only in an aqueous medium but also in other solvents and then provide stabilizing and templating effects for NP preparation.[76] ILs and SAILs are useful in introducing anisotropy in NPs[77] by differential capping of the ions and providing a surrounding medium of distinctive viscosity and surface tension that affects the rate of nucleation and growth of NPs and their resulting properties.[78,79]

With the passage of time, novel approaches are being proposed involving minimum use of chemicals to achieve the desired product in a facile manner. Keeping these considerations in mind along with the limitations of the conventional methods and the novelty brought by ILs in the fields of organic synthesis, catalysis, and nanotechnology, this feature article covers the synthesis and utilization of different ILs and SAILs for the preparation of a variety of nanomaterials (mixed ferrites, ferrites, noble metal and noble metal based NPs) followed by their conjugation with 2D materials (graphene and MoS_2) exfoliated *in situ*, for enhanced photo-catalysis in a sustainable manner under visible light or sunlight (Scheme 1).

The future scope of ILs, SAILs and similar solvents in the area of material science is discussed thereafter. It is expected that this article will offer a new perspective to design efficient, benign and novel approaches in the field of nanoscience and nanotechnology employing ILs or SAILs for diverse applications not limited to photocatalysis but for futuristic applications such as value addition to CO_2, photocatalytic water splitting, solar fuel cells and batteries, and biological applications in bioreactive sensors and drug delivery systems.

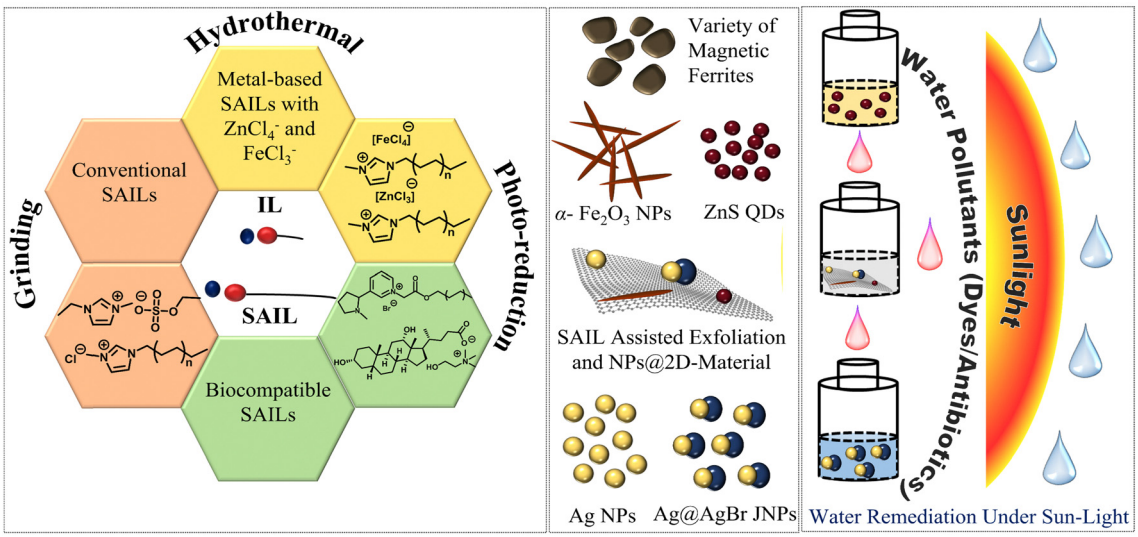

Scheme 1 IL and SAIL-assisted preparation of a variety of NPs, their composites, and catalysis for water remediation.

Utility of ILs for the preparation of NPs

The primary approach of using ILs in NP synthesis involves ILs as mere solvents or a support for the immobilization of particles. Owing to exceptional characteristic properties shown by hollow nanostructures, Sun *et al.*[80] reported a general template-engaged synthesis of hollow metal nanoparticles with size and shape dependent on the sacrificial core template using ILs. Nakashima *et al.*[81] reported for the first time the interfacial synthesis of hollow TiO_2 microspheres using imidazolium-based IL, $[C_4mim][PF_6]$. Liu *et al.*[82] prepared ZnSe hollow nanospheres with the help of task-specific Se-functionalized IL, which not only acted as a stabilizer but also the precursor of Se for the reaction. The reaction conditions contained hydrazine (N_2H_4) as the reductant and N_2 bubbles to induce the synthesis of hollow particles. Zhang *et al.*[28] utilized carboxylic acid and amino acid functionalized ILs as capping agents to prepare gold (Au) and platinum (Pt) NPs. The limitation of this approach is the use of pre-synthesized Au and Pt seeds prepared by chemical reduction employing sodium borohydride. IL-functionalized NPs were further utilized as heterogeneous catalysts in organic synthesis. Polyvinylpyrrolidone (PVP)-copolymerized IL-supported Pt NPs were synthesized by Yuan *et al.*,[83] for the hydrogenation of chloro–nitro compounds to chloro-amines with high selectivity. Scheeren *et al.*[84] reported the synthesis of Pt(0) NPs stabilized by imidazolium-based IL in the presence of molecular hydrogen as the reductant. Electroless preparation of Pt NPs using IL as capping agents containing $[NTf_2]^-$ anion has also been reported where the length of the alkyl chain was found to control the size of the NPs.[85] In a similar approach, palladium (Pd) NPs were prepared by Yu *et al.*,[86] using imidazolium-based IL-copolymer support for the Suzuki–Miyaura reaction showing high durability and activity. The templating effect of imidazolium-based ILs has also been established by the IL-assisted synthesis of Au NPs,[87] binary nanoparticles by the sputtering method,[88] and Au nano-sheets at the IL/water interface prepared by photo-irradiation.[89] Semiconductor nanocrystals have been stabilized by ILs, which in turn affect the structural and catalytic properties of the prepared NPs.[57,90,91] Getting known for their interesting properties and tunability, researchers further started utilizing ILs for roles other than solvent media in NP synthesis.

The surface activity of SAILs was exploited for the synthesis of IL-capped AgBr nanocrystals with size and shape controlled by alkyl chain length of the IL *via* a hydrothermal method by Lou *et al.*[92] The stabilizing ability of SAILs is believed to be due to their surface activity, which lowers the surface tension, viscosity, and dielectric constant of the surrounding medium resulting in slow Ostwald ripening and hence, fast nucleation and slow aggregation leading to small-sized NPs. In the case of metal NPs, ionic head groups of SAIL tend to interact with the metal ions and direct the reduction and growth of the NPs.[93,94] Thus, ILs and SAILs form a useful class of new solvents for providing a template to the NPs in relatively less toxic reaction conditions with minimal use of chemical reagents to carry out the reaction. The forthcoming sections cover IL or SAIL-assisted sustainable preparation of a variety of NPs and their heterostructures with 2D (graphene and MoS_2)-materials majorly reported by our research group for their photocatalytic applications.

Preparation of nano ferrites employing SAILs

Perovskite-type rare earth ortho ferrites, generally represented as $RFeO_3$, where R is a rare earth metal that crystallizes in a perovskite structure with Fe^{3+} ions surrounded by six oxygen ions giving octahedral coordination, have a wide range of applications.[95–97] Lanthanum-based orthoferrites ($LaFeO_3$), which can be prepared by different synthetic routes,[98–100] are greatly exploited for their photocatalytic activity under visible light.[101] Super-exchange interactions between the Fe^{3+} ions through intervening O^{2-} ions in these ferrites result in anti-ferromagnetism.[102] Doping with cations enhances their magnetic as well as photocatalytic properties,[98,103–107] however the requirement of high annealing temperatures, poor homogeneity, high porosity, and a large distribution of particle size hinders their efficiency. Considering the above premises, we have reported the synthesis and characterization of $La_{0.9}Ce_{0.1}Fe_{1-x}Co_xO_3$ NPs using an imidazolium-based SAIL, 1-hexadecyl-3-methylimidazolium chloride, $[C_{16}mim][Cl]$, as a soft template for shape and size control *via* the hydrothermal method for the first time (Fig. 1).[108] $[C_{16}mim][Cl]$ used for the capping of the ferrite NPs seems to play an important role in controlling the shape and size of the NPs. A strong tendency of $[C_{16}mim][Cl]$ to self-assemble into ordered structures above its critical micelle concentration (cmc $\sim$ 1 mM)[109] accounts for inducing anisotropy and directing the growth of ferrite NPs into elongated rod-like nanocrystals. Increase in concentration of SAIL (0 mM to 200 mM) resulted in asymmetrical elongated rod-like NPs in contrast to nearly symmetrical NPs in the absence of SAIL. The content of the Co-dopant also affected the shape owing to interactional alterations between the cationic head group of SAIL and metal ions. The induced structural anisotropy also affected the magnetism and photosensitivity of the nanoferrites, expected to be useful in various applications.

The effect of the type of dopant was further probed by doping La–Ce ferrites with Mn^{2+} in place of Co^{2+} to prepare $La_{0.9}Ce_{0.1}Fe_{1-x}Mn_xO_3$[110] adopting a similar approach using $[C_{16}mim][Cl]$ at a fixed concentration of 50 mM, which was higher than the reported cmc of the SAIL.[109] In the presence of a SAIL micellar template, directional growth was favored leading to the formation of elongated rod-like structures. An increase in the concentration of the dopant, from x = 0 to x = 0.3, led to a shift from weak ferromagnetism to paramagnetism (Fig. 2), which also prevented agglomeration. The results obtained from Mössbauer studies were also found to be in accordance with the effect of the amount of Mn-doping on the magnetic and hence structural properties of the prepared nano-ferrites (Fig. 2). The appearance of a central doublet in the Mössbauer spectra with increasing amount of Mn-doping corresponds to the paramagnetic behavior of the NPs depending on the particle size. With smaller crystallite size, elongated rod-like morphology, and more surface exposure,

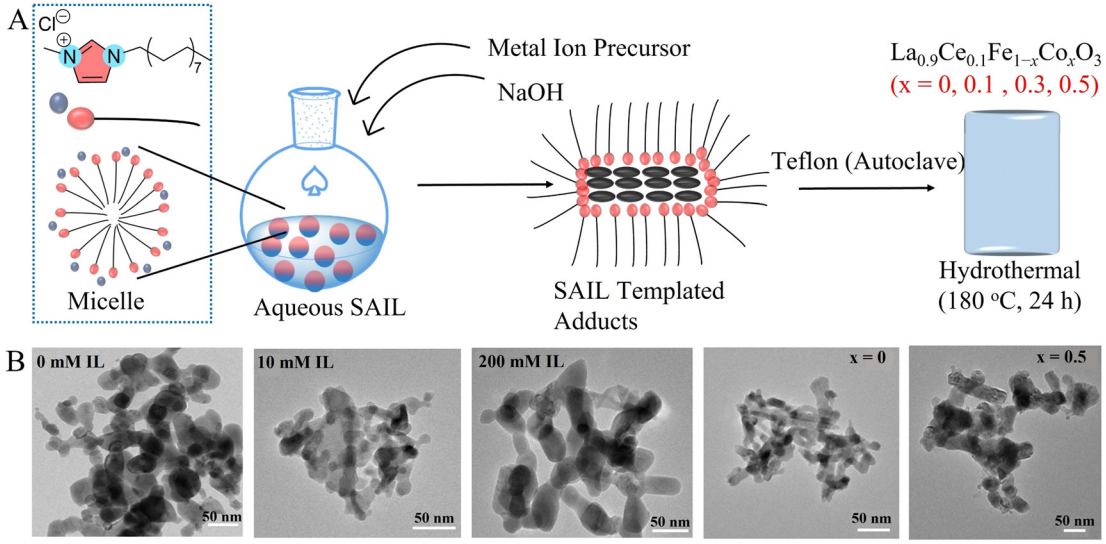

Fig. 1 (A) Schematic representation of the synthesis of $La_{0.9}Ce_{0.1}Fe_{1-x}Co_xO_3$ NPs; and (B) variation in morphologies of the NPs with changes in concentration of IL from 0 mM to 200 mM, and with change in dopant concentration as x = 0 and x = 0.5. Adopted from ref. 108 with permission. Copyright 2015 The Royal Society of Chemistry.

these nano-ferrites are expected to be highly efficient in various photosensitive applications.

Another substitute for Fe^{3+} ions for doping of La–Ce ferrites is Cr, due to its existence in multiple oxidation states dependent upon different methods followed for the preparation of ferrites. Super-exchange interactions between Fe^{2+} and Cr^{2+} ions are known to take place in the ordered B-site resulting in enhanced magnetic properties of the formed nanoferrites.[111] Cr-doped La–Ce nano-ferrites were already reported,[106] before our group exploited the surface active properties of SAIL, $[C_{16}mim][Cl]$, for the hydrothermal synthesis of the Cr-doped nano-ferrites and investigated their magnetic and optical properties.[112] The concentration of Cr doped in $La_{0.9}Ce_{0.1}Fe_{1-x}Cr_xO_3$ ferrites was found to affect the crystallite size of the NPs, which first decreased with an increase in the concentration of dopant from x = 0 to x = 0.3, but then increased at x = 0.5 because of the formation of a secondary phase of La_2CrO_6. Here, the SAIL was found to be responsible for the formation of La_2CrO_6 along with the desired nano-ferrites.

At low content of Cr-doping, directional growth was observed leading to the formation of rod-like structures of nano-ferrites. At higher concentrations, an increase in magnetism increased the rate of agglomeration of the particles, which ultimately resulted in thick rods with induced branching in the nano-ferrites. Magnetic behavior was also prominent at low concentrations, but a decrease in magnetism was observed at higher dopant concentration (x = 0.5).

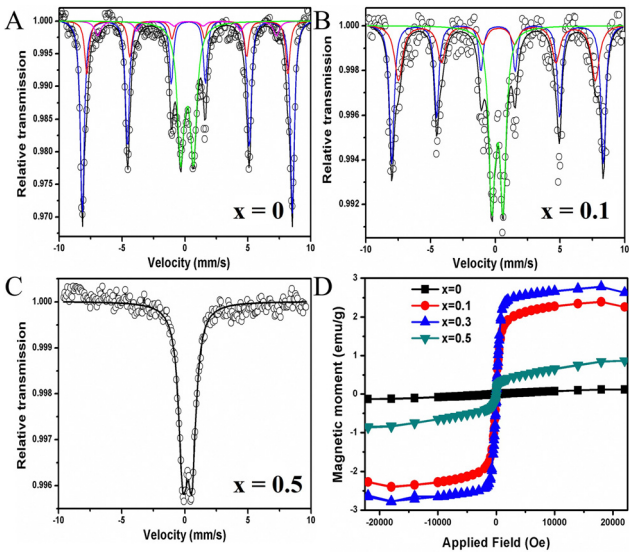

Fig. 2 (A)–(C) Mössbauer spectra; and (D) hysteresis loops of the prepared $La_{0.9}Ce_{0.1}Fe_{1-x}Mn_xO_3$ NPs employing $[C_{16}mim][Cl]$ (50 mM) *via* a hydrothermal method. Adopted from ref. 110 with permission. Copyright 2017 Elsevier B.V.

IL-assisted preparation of α-Fe_2O_3 NPs

Iron-based nanomaterials have been frequently utilized in various applications owing to their great magnetic and optical properties.[113–115] The high stability, economic viability, and non-toxic nature of α-Fe_2O_3 NPs attract great scientific attention.[116] Size and shape control in α-Fe_2O_3 NPs has been achieved by different methods resulting in the formation of nanotubes and nanorods,[117] nanocubes,[118] flower-shaped NPs,[119] and nanodiscs.[120] However the consumption of time, use of VOSs and high energy input in multistep reactions limit the viability of the reported methodologies. Various hydrothermal synthetic approaches have been reported for the preparation of hematite nanocrystals for different applications,[121–123] but utilization of IL to prepare iron oxide nanocrystals was scarcely reported,[124] which could be related to the high cost of preparation of neat ILs. Thus, solutions of ILs in different solvents were encouraged.[125]

Binary mixtures of ILs with polar solvents offer interesting dynamics for affecting the interactions responsible for size control and structural orientation of NPs. The energetics and structure of the binary mixture of 1-ethyl-3-methylimidazoliumethylsulfate, [C_2mim][C_2OSO_3] and water were studied by volume, density, and viscosity studies, which explain the segregation of IL in the IL-rich and water-rich regions, respectively.[126–128] Inspired by the presence of bi-continuous structures in binary mixtures of IL with water, our group has introduced a greener approach to prepare photosensitive α-Fe_2O_3 NPs in binary mixtures of 1-ethyl-3-methylimidazoliumethylsulfate, [C_2mim][C_2OSO_3] and ethylene glycol (EG)[129] *via* simple grinding while avoiding high-pressure conditions. The effect of IL on the structural, magnetic, and optical properties of the NPs was examined by varying the percentage of IL in the binary mixture from 0 to 25, 50, 75, and 100% (Fig. 3). H-bonding interactions between the cationic head group of the IL with –OH groups of EG, and differential aggregation behavior, depending on the content of IL in the binary mixtures, accounted for the stabilization and affected the characteristic properties of the formed hematite NPs (Fig. 3).

Easy preparation avoiding any sophisticated instrument added to the economic considerations of the proposed synthetic route. It was observed that dispersion forces dominate in the mixture, but with an increase in the content of IL, the interactions between IL and EG are compensated by increased interactions of constituent ions of IL and EG with the Fe^{3+} ions and α-Fe_2O_3 NPs. This led to greater capping by the IL and restricted growth of the particles, resulting in decreased crystallite size of the NPs with the increase in IL concentration (Fig. 4). The structural, optical and magnetic properties of the prepared α-Fe_2O_3 NPs were investigated (Fig. 4).

Due to forbidden d–d transitions and lattice relaxations, α-Fe_2O_3 in the bulk form does not exhibit luminescence.[130] However, tuning the size of particles to the nano-size range results in a quantum confinement effect along with reduced magnetic interactions and loss of long-range order, leading to the emission of luminescence by the NPs.[131] The characterization of the prepared α-Fe_2O_3 NPs was done by Mössbauer spectroscopy where the appearance of a central quadrupole doublet along with the characteristic sextet, corresponds to the development of superparamagnetic behavior in the NPs with increasing IL content and decreasing crystallite size (Fig. 4).

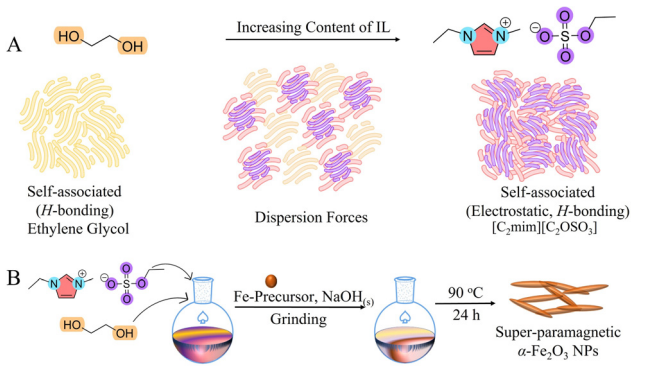

Fig. 3 (A) Interactive forces existing in binary mixtures of IL and EG at varying amounts of ILs; and (B) schematic representation of the procedure of synthesis of α-Fe_2O_3 NPs in IL-EG binary mixtures.

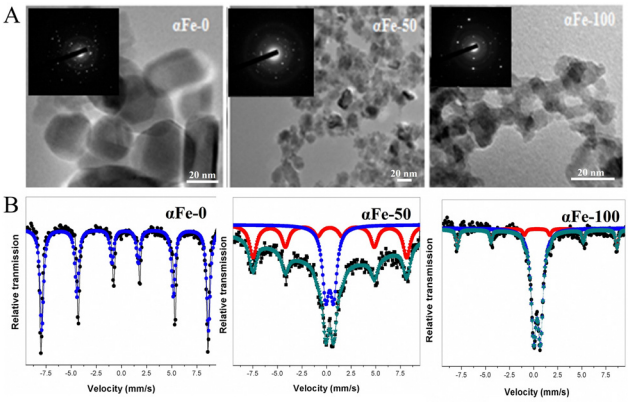

Fig. 4 (A) TEM images; and (B) Mössbauer spectra of α-Fe_2O_3 NPs prepared at different IL concentrations in an IL:EG binary mixture. 0, 50 and 100 in (A) and (B) represent the content of IL in the binary mixture, respectively. Adopted from ref. 129 with permission. Copyright 2015 The Royal Society of Chemistry.

A broader central doublet in the Mössbauer spectrum of α-Fe-50 than α-Fe-100 indicates a smaller crystallite size of the α-Fe-50 NPs.

Metal-based ILs for α-Fe_2O_3 NPs and ZnS QDs

The availability of metal ion precursor, solvent, and templating agent in a single benign component rather than three different entities would add to the sustainability of the preparation methods of nanomaterials. Here, metal-containing ILs (MILs) have received significant attention.[132] Our group reported Fe-based ILs, 1-alkyl-3-methylimidazolium tetrachloroferrates [$C_n$mim][$FeCl_4$] (n = 4, 8, 16), which were synthesized and utilized as the precursor, templating agent, and solvent for the preparation of α-Fe_2O_3 NPs for the first time (Fig. 5).[133]

Stoichiometric amounts of $Fe(NO_3)_3{\cdot}9H_2O$ and [$C_n$mim][$FeCl_4$] IL were mixed and ground in a pestle-mortar at room temperature (RT) in the presence of NaOH. The obtained paste was then washed, dried, and calcinated at 600 °C for 4 h to get the final product. α-Fe_2O_3 NPs were photo-catalytically active towards RhB degradation under sunlight. Although there were earlier reports concerned with IL-assisted preparation of α-Fe_2O_3 NPs *via* solvothermal or hydrothermal approaches,[134,135] the impact of the structural features of the MIL was never discussed in controlling the properties of α-Fe_2O_3 NPs. As mentioned in our work, the $FeCl_4^-$ ion is supposed to remain in close vicinity to the imidazolium head group and away from the hydrophobic alkyl chain. Thus, oxidation and nucleation of Fe^{3+} ions for the preparation of α-Fe_2O_3 were believed to take place in the polar domain of the bi-continuous assembly of the IL. This predominantly impacted the shape and size control of NPs by changing the alkyl chain length of the non-polar domain

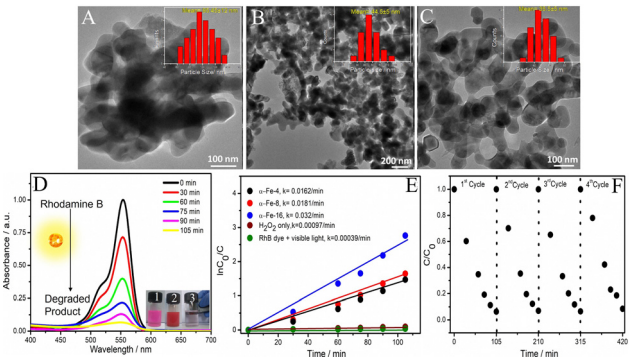

Fig. 5 (A)–(C) TEM images of α-Fe-4, α-Fe-8 and α-Fe 16, respectively (insets show their respective particle size distribution); (D) UV-vis absorption spectra of aq. RhB in the presence of α-Fe-16 under sunlight at different time intervals and corresponding images showing dye degradation; (E) rate of dye degradation and (F) recyclability of α-Fe-16 as a photocatalyst for 4 repeated catalytic cycles. Adopted from ref. 133 with permission. Copyright 2019 The Royal Society of Chemistry.

(Fig. 5). The prepared NPs (α-Fe-16) (16 represents the alkyl chain length of the MIL used) were able to decompose ~98% dye in 105 min under sunlight exposure, while the rate of dye degradation decreased with decreasing length of the alkyl chain of the MIL used for the preparation of NPs. Sunlight was necessary as the reaction did not take place under white light, which confirms the role of sunlight in conjunction with α-Fe_2O_3 NPs, owing to a large band gap of the prepared NPs.

Numerous methods are reported for the preparation of a variety of QDs,[6,47,131,136] but greener and more sustainable approaches are always looked upon for enhanced utilization of such materials in various applications. Our group was the first one to report[137] the preparation of ZnS QDs using Zn containing IL *via* a one-pot facile approach (Fig. 6).

The synthetic procedure involved mixing and grinding equimolar amounts of ZnS and 1-alkyl-3-methylimidazolium trichlorozincate [$C_n$mim][$ZnCl_3$] (n = 4, 8, 16) IL in a pestle-mortar to yield ZnS QDs (QD-C4, QD-C8, QD-C16, where 4, 8, 16 denote the alkyl chain length of the IL used). MIL plays three important roles in the preparation of the QDs, (i) providing a medium for the reaction to take place, (ii) acting as a precursor of Zn^{2+} ions for the reaction, and (iii) acting as a templating agent to control the size and shape of the QDs. The length of the alkyl chain of the IL affects the dielectric constant, viscosity, and surface tension of the medium. This in turn affects the rate of nucleation and rate of growth of the NPs and hence controls the rate of agglomeration and particle size thereafter. It was

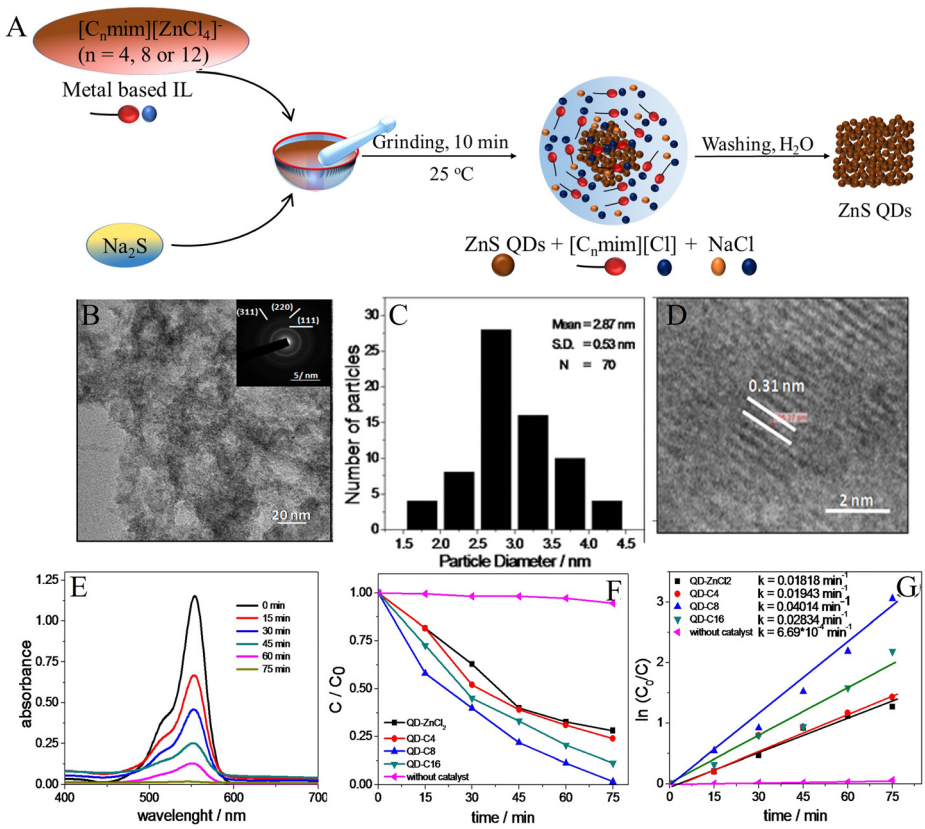

Fig. 6 (A) Schematic representation of the synthesis of ZnS QDs stabilized by [$C_n$mim][$ZnCl_3$]; (B) TEM image, (C) particle size distribution, (D) HR-TEM image showing lattice planes of ZnS QD-C8; (E) absorption spectra of an aqueous solution of RhB in the presence of QD-C8 exposed to UV irradiation for different time intervals; (F) photocatalytic performances of the different QDs and (G) comparison of the reaction rates together with the rate constants for the different QDs for degradation of RhB in aqueous solutions. Adopted from ref. 137 with permission. Copyright 2017 The Royal Society of Chemistry and the Centre National de la Recherche Scientifique.

observed that the smallest crystallite size forms in the case when $[C_{16}mim][ZnCl_3]$ MIL was used for the preparation of ZnS QDs. The segregation of polar and non-polar domains of the MIL was proposed to affect the size and shape of the QDs.

Optical properties of the ZnS QDs were found to be dependent on the particle size, as observed from the photoluminescence and photocatalytic studies. The prepared QDs were able to decompose rhodamine B dye in an aqueous solution under UV-light irradiation. The activity of the QDs followed an increasing trend with an increase in chain length of the employed MIL up to $n = 8$, owing to a decrease in the crystallite size. However, despite being the smallest in size, the probability of residual MIL and the highest band gap energy renders QD-C16 less efficient in photocatalysis as compared to QD-C8 (Fig. 6). QD-C8 showed maximal activity towards photodegradation of the dye with 100% degradation in 75 minutes.

Noble metal-based NPs employing SAILs

Local surface plasmon resonance (LSPR) is a property shown by noble metal NPs that makes them responsible for feasibly absorbing under visible or white light.[138] Thus noble metal-based NPs such as Au, Ag, and Pt NPs have got significant attention from the scientific community for photocatalysis and other photosensitive applications.[4,9,11,12,26,139] Tuning the large band gaps of semiconductor NPs with noble metal NPs not only helps in enhancing the photocatalytic efficiency but also offers photocatalytic stability to the nanocomposites (NCs) under visible light. For example, the conjunctions of Ag and Au noble metal NPs with TiO_2 resulted in enhanced photocatalytic activity, owing to efficient charge transfer from the surface plasmons of noble metal NPs to the conduction band (CB) of the semiconductor. This prevents charge recombination and encourages charge separation resulting in efficient photocatalytic efficiency.[7,140] Ag/AgX (X = Cl, Br, I) based NCs are quite popular as plasmonic photocatalysts, which absorb energy efficiently in the visible spectrum. Numerous reports are available in the literature concerned with the photocatalytic activities of Ag/AgCl, Ag/AgBr and Ag/AgI nanomaterials prepared by conventional methods using surfactants under relatively cumbersome reaction conditions.[141–143] Therefore, novel and sustainable approaches are required for the preparation of structurally anisotropic and visible light-active Ag/AgX NCs. Aqueous phase synthesis of Janus-shaped Ag/AgBr NPs stabilized by the cucurbit[n]uril macrocycle, where Ag^+ was reduced by electron beam irradiation, has been reported.[144] Kossak *et al.*[145] reported the aqueous phase synthesis of L-arginine-stabilized Ag/AgBr JNPs prepared by *in situ* photoreduction of a metal halide intermediate under UV irradiation. The employment of SAILs in stabilizing and inducing anisotropy in the synthesis of Ag/AgX nanomaterials was not reported until our group reported a facile one-pot synthesis of Ag/AgBr Janus-shaped NPs using a nicotinium cation-based SAIL under sunlight exposure within one minute of solar irradiance (Fig. 7).[146]

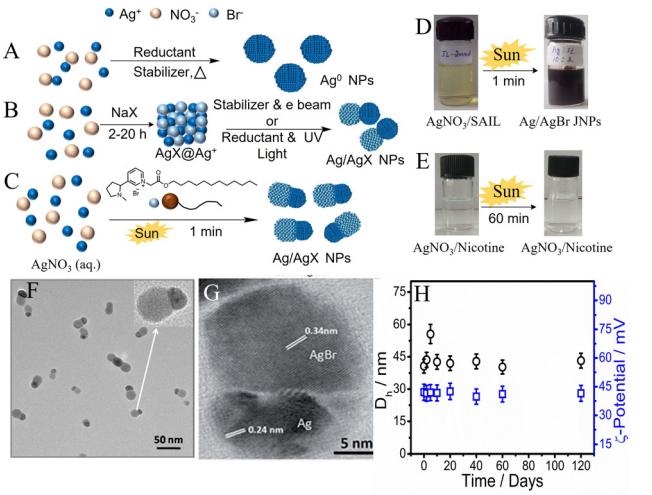

Fig. 7 (A) Conventional, (B) metal–halide mediated and (C) SAIL mediated strategies for the preparation of Ag@AgX NPs; (D) and (E) show the photographs of formation and non-formation of Ag@AgBr JNPs under different conditions, respectively; (F) TEM; and (G) HR-TEM images of Ag@AgBr JNPs; and (H) shows the variation of the hydrodynamic diameter (D_h) along with the ζ-potential of Ag@AgBr JNPs as a function of time when stored in the dark at 25 °C. Adopted from ref. 146 with permission. Copyright 2019 The Royal Society of Chemistry.

The economic and environmental viability of the procedure lies in the minimal use of chemicals as the SAIL used acts as the precursor for providing the Br^- ion required for the formation of AgBr, a templating agent for the capping of the NPs, and the reducing agent for the reduction of Ag^+ ions to Ag^0. The shape and size control by the SAIL were exquisite as distinguished multi-phased and highly stable Janus-shaped NPs (JNPs) were obtained with this methodology (Fig. 7). The SAIL concentration used for the JNP synthesis was below the reported cmc,[147] which means that SAIL provided the templating effect to the growing Ag@AgBr NPs in the monomeric form. The interactions of the photosensitive nicotinium cation with the Ag^+ ions on the AgBr surface resulted in *in situ* reduction and symmetry-breaking induced generation of Janus-shaped Ag/AgBr NPs under sunlight. The NPs were found to be photo-catalytically active for the efficient degradation of model water-pollutant such as RhB dye and reduction of 4-nitrophenol under sunlight with a relatively higher rate constant (Fig. 8). A series of Ag@AgBr NPs were synthesized employing varied concentrations of the SAIL and $AgNO_3$. However, the highest photocatalytic activity was shown by Ag/AgBr-1 JNPs (prepared by using $[AgNO_3]$ = 10 mM and [SAIL] = 2 mM), which showed distinguished structural anisotropy (Fig. 7). The Ag/AgBr-1 JNPs were able to degrade ∼100% of the RhB dye in 25 minutes of sunlight irradiation with a rate constant of 0.15 min^{-1} (Fig. 8). Here, we proposed a new sustainable approach for synthesizing photo-catalytically active nanomaterials with enhanced structural anisotropy using relatively greener alternatives. The novelty of the process lies in the non-requirement of separate reducing and capping agents, and complex media for precise shape and size control on the NPs.

Taking into consideration the applicability of NCs of noble metals with semiconductors, multicomponent NCs can be tried

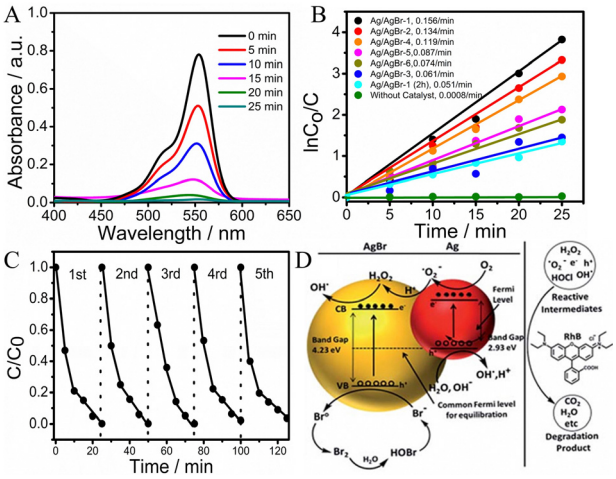

Fig. 8 (A) Time-dependent UV-vis absorbance spectra of an aqueous solution of RhB in the presence of Ag/AgBr-1 as a catalyst; (B) catalytic performances of different NPs and (C) recycling efficiency of the Ag/AgBr-1 catalyst for 5 repeated catalytic cycles; and (D) represents the plausible mechanism similar to that reported earlier and the band gap values of Ag/AgBr-1 JNPs mentioned in the scheme has been calculated using UV-visible measurements. Adopted from ref. 146 with permission. Copyright 2019 The Royal Society of Chemistry.

for their distinctive structural and morphological properties. Au–Ag@AgBr was first synthesized by the Au seed-mediated method using a high-intensity Hg lamp as the energy source with PVP acting as the capping and reducing agent in the presence of EG as the solvent.[148] Another group reported the synthesis of Au/Ag@AgBr NCs using CTAB as a capping agent and Au seed particles to induce nucleation and growth of the nanoparticles with insignificantly induced anisotropy.[149] Both reports explained the formation of AgBr on the pre-formed Au seeds in their respective environments, followed by *in situ* reduction of Ag^{+} to Ag^{0}. We were curious to understand the dynamics of stabilization of noble metal-based NCs assisted by surface-active agents, which lead to anisotropic growth of the particles. Our group reported the preparation of AuAg alloy@AgBr JNPs with precise shape and size control offered by CTAB as the capping agent in aqueous medium and reduction of the metal ions induced by a natural source, ascorbic acid, under sunlight exposure.[150] We achieved control over the morphology of the NPs by variation in the pH of the reaction medium. The viability of this report lies in the pH-dependent dissipative self-assembly of CTAB-stabilized AgBr colloids in a non-conventional top-down approach, leading to shape and size controlled by the interactions prevailing among the surfactant, metal ions and reducing agent in the reaction medium (Fig. 9). The synthesis involved the preparation of AgBr colloids stabilized by CTAB, followed by simultaneous reduction of Ag^{+} and Au^{3+} in the presence of sunlight. Precisely multi-phased Janus-shaped nanoparticles were observed from the TEM with size-dependent optical properties.

JNP-1 and JNP-2 were prepared under the same experimental conditions with a difference in pH of the medium (JNP-1 at pH $\sim$ 4.2 and JNP-2 at pH $\sim$ 9.4). The prepared Janus-shaped AuAg alloy@AgBr NPs were found to be photo-catalytically efficient in sunlight-driven degradation of RhB dye as a model pollutant (Fig. 10), and for bacterial growth inhibition with very low minimum inhibitory concentration ($\sim$35 μg mol^{-1}).

Hetero-nanocomposites of NPs with 2D materials (graphene and MoS_2) using SAILs

There have been numerous reports concerned with the conjunction of graphene oxide (GO),[151] and reduced graphene oxide (rGO) with other metals NPs,[152,153] for photocatalytic applications. Attempts have also been made to exploit the

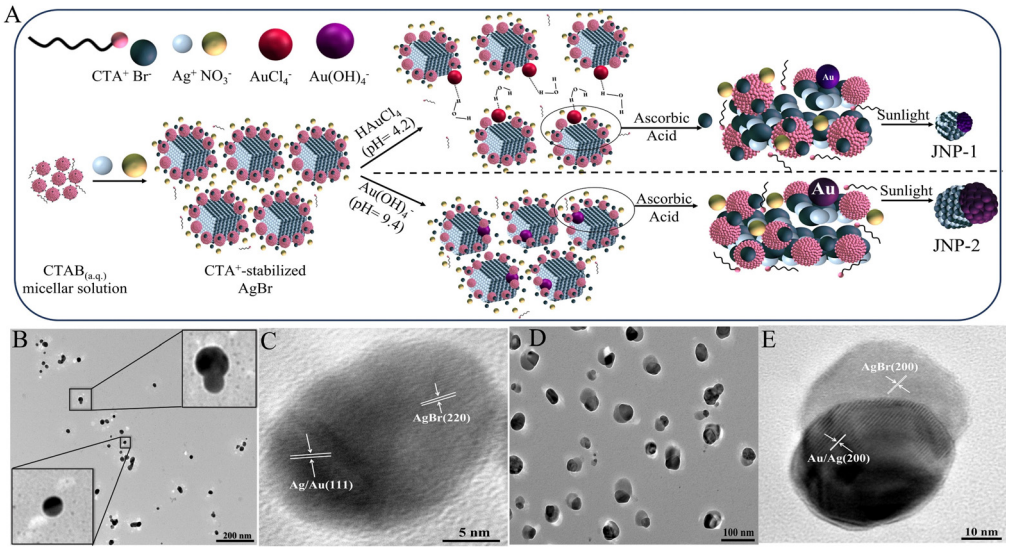

Fig. 9 (A) Diagrammatic representation of the mechanism followed during the preparation of JNP-1 and JNP-2; (B) and (C) TEM and HR-TEM images of JNP-1; and (D) and (E) TEM and HR-TEM images of JNP-2. Adopted from ref. 150 with permission. Copyright 2024 The Royal Society of Chemistry.

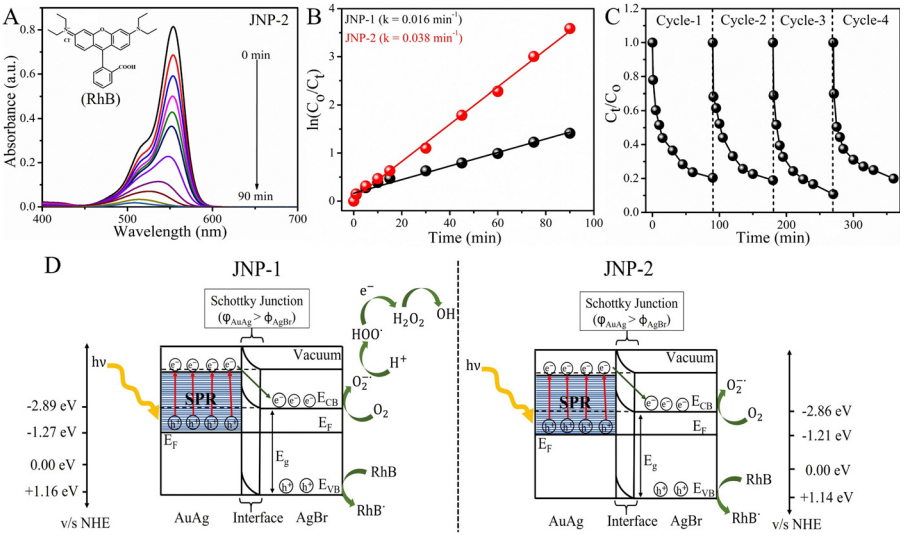

Fig. 10 (A) Time-dependent UV-vis absorbance spectra showing the degradation of RhB in the presence of JNP-2; (B) catalytic activities of JNP-1 and JNP-2; (C) recyclability of JNPs; and (D) schematic representation of the formation of charge carriers involved in the photocatalysis. Adopted from ref. 150 with permission. Copyright 2024 The Royal Society of Chemistry.

electrical properties of defect-free graphene in conjunction with other nanomaterials to design more efficient catalytic nanosystems.[154,155] Provoked by the well-established ability of surfactants to lower the surface tension of the medium and intercalate in between the layered 2D materials, our research group synthesized a metal-containing SAIL, $[C_{16}mim][FeCl_4]$, and employed the same for successful exfoliation of few-layered thick graphene flakes in aqueous medium *via* low-energy bath sonication.[156] Graphene flakes were obtained in good yield with negligible surface defects. The highly positive zeta potential value (+40.9 mV) and colloidal stability of exfoliated graphene up to 30 days confirm the potential of the SAIL-assisted exfoliation method. The exfoliated graphene flakes were found to be 2–4 nm thick corresponding to 3–12 layers of graphene. This was followed by *in situ* decoration of α-Fe_2O_3 NPs on the exfoliated graphene nanosheets by subjecting the aqueous dispersion of SAIL-stabilized graphene flakes, with [SAIL] = 50 mM, to microwave irradiation (Fig. 11). The crystallite size of the thus formed α-Fe_2O_3 NPs was found to be smaller than that obtained in the case of bare α-Fe_2O_3 NPs prepared under the same conditions but in the absence of graphene. The prepared NCs were tested for their photocatalytic efficiency in the degradation of an antibiotic sulfamethoxazole (SMX) under white light. Antibiotics such as SMX are harmful to the environment owing to their non-biodegradable nature and toxic impact on aquatic life. New materials are required for the successful decomposition of such types of harmful compounds in a facile manner. 92% SMX was degraded in 60 minutes when irradiated, followed by 59% and 3.3% by bare α-Fe_2O_3 NPs and graphene, respectively. The prepared NCs were found to be catalytically stable for up to 6 cycles. The probable reason behind the enhancement in photocatalytic activity of the α-Fe_2O_3 NPs when combined with graphene lies in the extensive surface area provided by graphene and the reduction

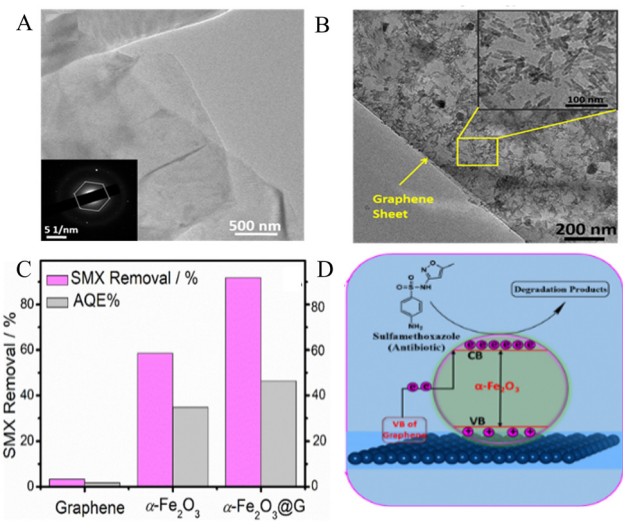

Fig. 11 (A) TEM image of an exfoliated graphene sheet; (B) TEM image of the prepared α-Fe_2O_3@G NCs; (C) photocatalytic antibiotic sulfamethoxazole (SMX) degradation efficiency of graphene, α-Fe_2O_3, and α-Fe_2O_3@G and their corresponding apparent quantum efficiencies (AQEs) under visible light; and (D) schematic representation showing the possible mechanism for electron transfer for the degradation of SMX antibiotic. Inset of (A) shows the SAED pattern of exfoliated graphene sheets. Adopted from ref. 156 with permission. Copyright 2020 The Royal Society of Chemistry and the Centre National de la Recherche Scientifique.

in charge recombination which results in efficient electron–hole pair separation and decreased band gap energy (Fig. 11). The most probable role of graphene in this NC is to photosensitize α-Fe_2O_3 NPs by donating electrons to the conduction band of α-Fe_2O_3 as also similarly described in the case of TiO_2@G NC.[155]

Another type of semiconductor-graphene NC reported by our group was ZnS@G (Fig. 12). The low-energy bath sonication

exfoliation of graphene in aqueous medium assisted by surface-active Zn-containing SAIL, $[C_{16}mim][ZnCl_3]$ followed by *in situ* decoration of ZnS QDs results in ZnS@G NCs for photocatalytic applications.[157] The exfoliated graphene flakes were 0.5–1 nm in height and up to 5-layered thick with negligible lattice defects. *In situ* decoration of graphene flakes with ZnS QDs was done in the aqueous colloidal dispersion of graphene having 50 mM $[C_{16}mim][ZnCl_3]$. It was mixed with equimolar amounts of Na_2S and subjected to magnetic stirring for 30 minutes at room temperature to obtain the ZnS@G NCs. The band gap calculated from the Tauc plot showed a decrease from 3.45 eV for ZnS QDs (prepared under the same reaction conditions in the absence of graphene) to 3.09 eV for ZnS@G NCs. Lowering of the band gap of ZnS@G NCs was attributed to the graphene, which prevented the electron–hole recombination and resulted in an increased electron density in the CB of ZnS, responsible for the enhancement of the photocatalytic activity of the NCs in visible light. Photoluminescence quenching observed in the presence of graphene confirmed the role of graphene in preventing electron–hole pair recombination. The prepared ZnS@G NCs were able to degrade RhB dye completely and antibiotic ciprofloxacin (CIP) under sunlight exposure, showing better catalytic activity than bare ZnS QDs reported earlier[137] which were photo-catalytically active in UV light (Fig. 12).

Although the activity of Ag/AgBr NPs was significantly enhanced compared to that of both Ag and AgBr NPs, their conjunction with 2D materials such as graphene is a field of interest. Prompted by the heterojunction formation between graphene and NPs supported by a large surface area of graphene, we combined the photocatalytic properties of Ag/AgBr NPs with a large surface area of graphene in a two-step one-pot sustainable strategy. Arora *et al.*[158] employed a nicotinium-based $[C_{12}ENic]$-[Br] SAIL, reported earlier[147] by our group, for exfoliation of graphene in an aqueous medium, followed by *in situ* decoration of Ag/AgBr JNPs on the exfoliated graphene sheets (Fig. 13) under sunlight. Not only this, the conjugated Ag/AgBr@graphene NCs showed enhanced photocatalytic efficiency under sunlight. Maximum exfoliation of graphene was achieved at [SAIL] = 10 mM, near to its cmc,[147] which points towards the dominance of the monomeric form of SAIL in graphene exfoliation. Graphene sheets of 2.4 nm thickness were obtained *via* low-energy bath sonication in good yield with negligible lattice defects and appreciable colloidal stability for up to 15 days as observed by a highly positive zeta potential value (+35.5 mV). The same SAIL-stabilized aqueous dispersion of graphene was used for *in situ* generation of Ag/AgBr JNPs, after diluting it to get a final SAIL concentration of 2 mM as it was reported to produce Ag/AgBr JNPs with effectively induced symmetry-breaking under sunlight.[146] As discussed earlier,

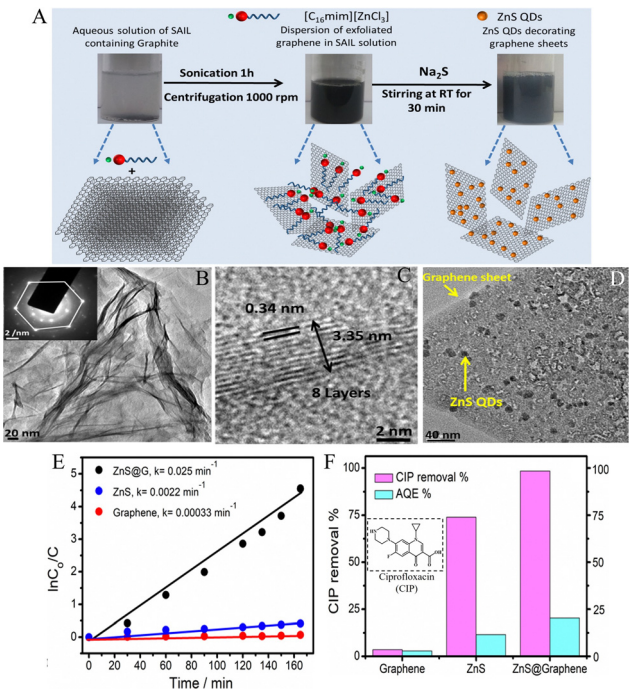

Fig. 12 (A) Schematic representation of exfoliation of graphene and subsequent preparation of ZnS QD decorated graphene; (B) TEM and (C) HR-TEM images of an exfoliated graphene sheet; (D) TEM image of the prepared ZnS@G NCs; (E) catalytic performances of ZnS@G, ZnS and graphene and their rate constants; and (F) photocatalytic CIP removal % of graphene, ZnS and ZnS@G catalysts and their corresponding apparent quantum efficiencies (AQE) under visible light. Inset of (A) shows the SAED pattern of exfoliated graphene sheets. Adopted from ref. 157 with permission. Copyright 2020 The Royal Society of Chemistry.

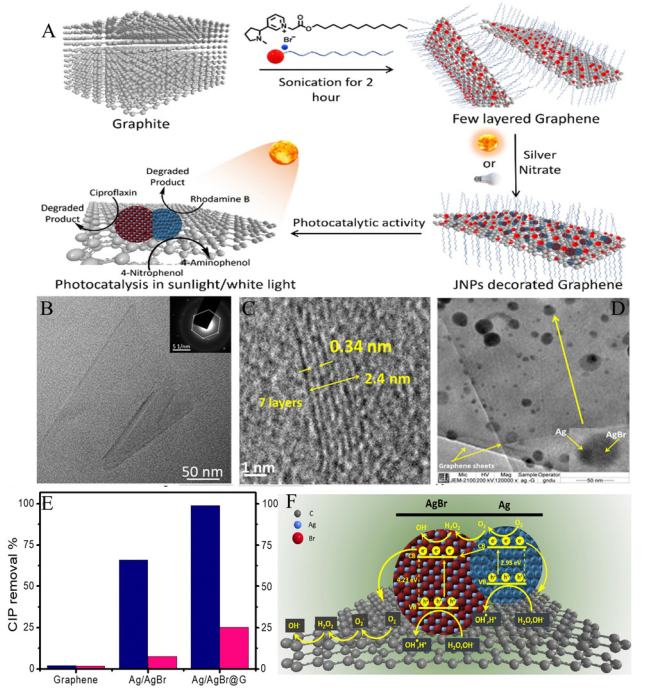

Fig. 13 (A) Schematic representation for *in situ* preparation of Ag/AgBr@G NCs and its photocatalytic activity; (B) TEM and (C) HR-TEM images of an exfoliated graphene sheet; (D) TEM image of Ag/AgBr@G NCs; (E) photocatalytic efficacy for the photodegradation of CIP and their corresponding apparent quantum efficiency (AQE%) using Ag/AgBr@G NC and their counterparts; and (F) plausible mechanism for the photocatalytic activity of Ag/AgBr@G NCs. Inset of (A) shows the SAED pattern of exfoliated graphene sheets. Adopted from ref. 158 with permission. Copyright 2021 Elsevier B.V.

[C_{12}ENic][Br] SAIL reduces Ag^+ to Ag^0 in less than 1 minute of sunlight exposure but in the presence of graphene, around 5 minutes were taken for the growth of Ag/AgBr@G NCs at the desired concentration. This was assigned to the reduced exposure of Ag^+ ions towards sunlight because of the presence of graphene sheets which slowed down the rate of reduction and growth of the NPs. The prepared NCs were able to decompose 99% of ciprofloxacin within 120 minutes of light exposure as determined by HPLC measurements. Moreover, the rate of photocatalysis was enhanced by 2–3 fold for the degradation of RhB dye and 4-NP by Ag/AgBr JNPs in the presence of graphene. Enhanced photocatalytic activity and stability of the prepared Ag/AgBr@G NCs are attributed to the presence of graphene as an electron-accepting agent in conjunction with Ag/AgBr, which assists in electron–hole separation and charge transfer, along with providing extended surface area for adsorption of reactant molecules.

Progress in graphene exfoliation has led to the exploration of other 2D materials with interesting properties. Transition metal dichalcogenides (TMDs), with a general formula of MX_2 (where, M is a transition metal and X = S, Se, Te), cover a wide range of materials for electronic and catalytic applications.[14] The exfoliation of bulk TMDs into 2D nanosheets would account for enhancement in their structural and electronic properties owing to the quantum confinement effect.[131] There have been reports of the conjugation of TMD nanosheets with other metal NPs for various applications.[24,159,160] Our group reported exfoliation of MoS_2 sheets assisted by a biological surfactant, choline deoxycholate [Cho][Doc], followed by *in situ* decoration with Ag NPs in a facile and sustainable manner.[161] Maximum exfoliation of MoS_2 was achieved by using 3 mM of [Cho][Doc] in an aqueous medium and then Ag@MoS_2 NCs were prepared at different concentrations of [Cho][Doc] and characterized for their morphological and optical properties. We were able to exfoliate 2–8 nm thick sheets of MoS_2 with good colloidal stability for at least 16 days. The *in situ* generation of Ag NPs took place under sunlight *via* $[Cho]^+$ induced reduction of Ag^+ to Ag^0 and the NPs capped by [Cho][Doc] (Fig. 14).

The size of the NPs was found to decrease with increasing concentration of [Cho][Doc] used in the preparation (10, 50 and 100 mM). The interaction of Ag NPs with MoS_2 seems to be reduced at high concentrations of the surfactant. At higher concentrations of [Cho][Doc], the number of free micelles increases and Ag^+ ions orient towards the negatively charged [Cho][Doc] micelles and not with the monomers intercalated among the MoS_2 sheets. Hence, more of the free Ag NPs are observed when 50 mM [Cho][Doc] is used, in contrast to the appreciable amount of Ag@MoS_2 NCs observed in the case of 10 mM [Cho][Doc] used. Thereafter, the photocatalytic efficiency of Ag@MoS_2(10) towards the degradation of RhB under sunlight was observed to be the best among all other NCs prepared. The photocatalytic efficiency of the NCs is attributed to the involvement of reactive oxygen species in oxidizing the organic dye (RhB) in the aqueous medium under sunlight. The NCs were found to be catalytically stable for up to 5 cycles with unaltered activity.

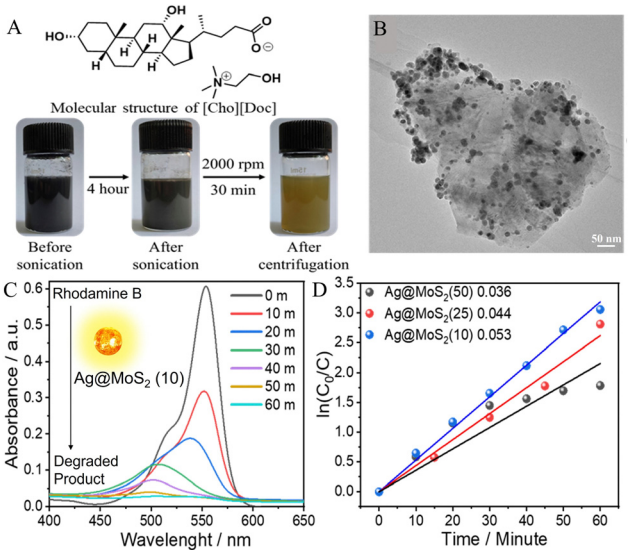

Fig. 14 (A) Molecular structure of [Cho][Doc] and exfoliation of MoS_2 in aqueous [Cho][Doc]; (B) TEM image showing Ag NPs adhered to the MoS_2; (C) time-dependent UV absorbance of RhB in the presence of Ag@MoS_2(10) under sunlight; and (D) comparison of the kinetics of Ag@MoS_2(10) NCs, Ag@MoS_2(25) NCs and Ag@MoS_2(50) NCs. Adopted from ref. 161 with permission. Copyright 2024 Elsevier B.V.

Summary and outlook

This feature article presents our work focused on the synthesis of a wide range of ILs and their applications for the preparation of various magnetic and photocatalytic nanomaterials. Precise control of the particle size and directional growth of nanoparticles is governed by the structural properties of the ILs used. Pioneer works involved the use of ILs as a solvent in hydrothermal or sol–gel preparation methods of NPs. The study of self-assembled structures and distinctive aggregation behavior of ILs in aqueous medium has triggered the onset of IL engagement for the capping of NPs. The effect of IL on the viscosity, surface tension, and dielectric constant of the medium of the reaction has been found to be responsible for the rate of nucleation and Ostwald ripening in the synthesis of NPs. In addition to those qualities, some ILs with the ability to reduce interfacial tension, *i.e.*, SAILs,[68–73] have found their way in stabilizing colloidal dispersions of NPs. We have summarized the IL-assisted preparations of different transition metal-doped perovskite-type orthoferrites ($LaFeO_3$)[108,110,112] and hematite (α-Fe_2O_3) nanoparticles,[129] and investigations of their optical and magnetic properties. In order to make the preparation methodologies more hassle-free and chemical-free, we synthesized metal-based ILs (MILs), which not only stabilize the NPs by the self-aggregation behavior of the amphiphilic part, but the counterion also provides the metal precursor required for the NP formation. The use of MILs in the preparation of metal NPs reduces the number of chemical reagents required in controlling the kinetics and hence, the size of the NPs. Hematite NPs (α-Fe_2O_3)[133] and ZnS QDs[137] were synthesized from imidazolium-based Fe and Zn-containing ILs, respectively, showing photoluminescent behavior. These types

of task-specific ILs have achieved great success in nanotechnology for acquiring qualities specifically relevant to a particular chemical response. We also exploited the surface activities of the synthesized MILs in achieving successful liquid-phase exfoliation of graphene into few-layered thick nanosheets and subsequent *in situ* decoration with α-Fe_2O_3 NPs[156] and ZnS QDs,[157] respectively. In comparison to conventional methods reported earlier for the exfoliation of graphene and its derivatives, the use of SAIL-assisted exfoliation in aqueous medium driven by low-energy ultrasound waves seems to be more benign and sustainable. However, there is still a long way to go to achieve single-layered 2D materials employing SAILs. Furthermore, tuning of the electrical conductivity of graphene with optically active NPs helps in the efficient photogeneration of charge carriers responsible for the visible-light activity of the prepared NCs in various photocatalytic reactions.

The journey of finding new ways of synthesizing more efficient and sustainable ILs does not end. We have reported the synthesis of a functionalized SAIL based on nicotinium cation,[147] and its application in the sunlight-driven preparation of Ag/AgBr JNPs with induced symmetry-breaking induced by the templating effect of the SAIL in aqueous medium.[146] The economic and environmental viability of this work lies in the minimal use of harsh chemical reagents and energy sources to carry out the synthesis of anisotropic Ag/AgBr JNPs with enhanced photocatalytic activity. The photocatalytic activity of these NPs has been found to be better than bare Ag and AgBr NPs, respectively, owing to Fermi-level equilibration of electronic bands of Ag and AgBr as well as striking anisotropy in the shape control in the JNPs. The same SAIL has also been reported to be efficient in exfoliating graphene (G) nanosheets in aqueous medium *via* bath sonication and *in situ* decoration of Ag/AgBr JNPs onto exfoliated G to form Ag/AgBr@G NCs.[158] The band gap tuning by conjunction with graphene leads to enhancement in photocatalytic efficiency compared to the previously prepared bare Ag/AgBr JNPs. The templating effect of surface active agents in controlling the shape and size of the nanoparticles has been explained by our group in a recent report on the synthesis of CTAB-stabilized AuAg alloy@AgBr JNPs reduced by ascorbic acid in sunlight.[150] Dissipative self-aggregation behavior of CTAB micelles owing to the metal-surfactant interactions at different pH seems to induce symmetry-breaking and anisotropy in the Janus-shaped NPs, also affecting their photocatalytic and antibacterial properties. The impact on the optical properties of noble metal NPs in multicomponent NCs such as these open doors to new combinations of metal–semiconductor NCs for their band gap tuning and photosensitivity in visible light. We have summarized the preparation of Ag@MoS_2 NCs stabilized and reduced by a bio-based surfactant [Cho][Doc] in an aqueous medium under sunlight irradiation.[161] The surfactant was used for liquid phase exfoliation of MoS_2 nanosheets followed by *in situ* reduction of Ag NPs on the 2D nanosheets to form the photocatalytically active Ag@MoS_2 NCs. The area of research concerned with the sustainable development of various nanomaterials assisted by ILs is not limited but continues to grow with novel methodological approaches introduced with the discovery of new ILs. The collaboration of the fields of SAILs and nanotechnology seems to be highly anticipated and a successful one for those involved in the development of new methodological approaches for sustainable photocatalytic systems to cater to the needs of alternate energy sources, such as to harvest energy sources such as sunlight. The conversion of solar energy into thermal energy to provide the activation energy for up-hill reactions has been successfully employed in organic synthesis.[162,163] Plasmon heating and the generation of charge carriers on the absorption of solar energy account for the enhancement in the rate of reactions, adding to the sustainability and feasibility of the processes.[164] There are distinctive nanomaterials, 2D materials, metal nanoparticles and their composites available, and their photosensitive properties have been employed in organic synthetic reactions by harvesting light energy into chemical energy.[4,165–167] The advent of photocatalytic nanomaterials for organic reactions marks the transformation of conventional complicated approaches to relatively greener ones for the preparation of organic molecules of commercial importance. We aim to design more photosensitive and competent nanomaterials with precise size and morphological control using greener reagents and reaction conditions and to utilize them in significant photocatalytic processes (Scheme 2).

The Ag/AgX nanoparticles are well-known photocatalysts owing to the light-sensitive nature of AgX as already discussed. The excellent photocatalytic abilities of AgCl and AgBr have inspired the scientific community to design and investigate the properties of mixed halides. Ternary silver halides ($AgCl_xBr_{1-x}$) are known to have optical properties and photosensitivity depending on the composition of the material.[168] Numerous reports are available in the literature concerned with the synthesis of $AgCl_xBr_{1-x}$ NPs and investigating their optical properties for photocatalytic applications.[169–171] *In situ* generation of Ag@$AgCl_xBr_{1-x}$ NCs has been reported recently for improved photocatalytic activities.[172–174] However, the methods available

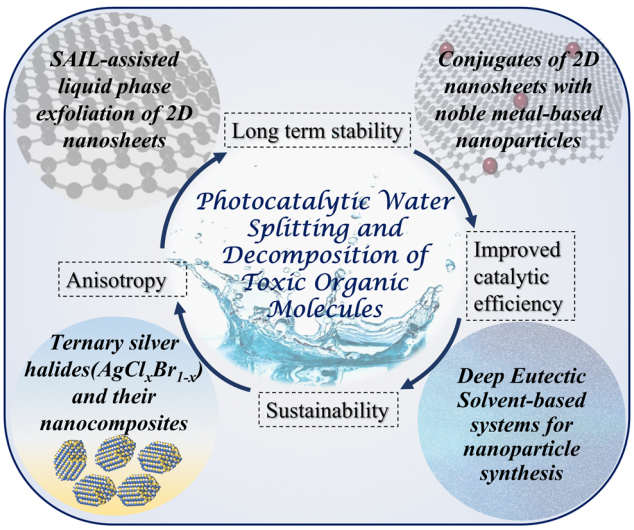

Scheme 2 Future perspectives for IL-assisted preparation of nanomaterials and their applications.

to date for the synthesis of $AgCl_xBr_{1-x}$ based NCs include the use of surfactants and non-polar solvents to ensure proper diffusion and anion exchange in the AgX lattice for finely tuned halide composition in the lattice for the required properties. Our group aims to design greener methodologies based on IL-assisted capping and reaction media for improved photocatalytic efficiencies of such NCs along with the pre-requisite requirement of size and shape control by using SAILs.

Moreover, 2D nanomaterials are gaining sufficient attention in the field of photocatalysis. The long-term stability of photocatalytically active materials when combined with 2D materials can be enhanced by immobilizing such materials into a hydrogel using a SAIL.[175] Such systems pave the way for synthesizing catalytic nanomaterials and storing them in the form of catalytic gels for long-term durability and stability. Despite of popularity of ILs in various fields of research, some limitations are encountered in the synthesis and applications of ILs, and more green alternative solvents are coming into the frame. These are called deep eutectic solvents (DESs). DES is a mixture of two components bound by H-bonding interactions (one component is an H-bond donor and the other is an H-bond acceptor) with properties different and a lower melting point from the individual components.[176] Ever since the onset of DESs, there has been remarkable interest in utilizing them in various applications.[177] DESs have proven to be better alternatives for solvents in reaction media owing to their facile synthesis and environment-friendly nature. Our group has used a metal-based DES in the dissolution of polymeric materials and investigation of the regenerated material for its structural and chemical properties.[178,179] We expect that the exquisite physical properties of DESs can be employed to test their ability to stabilize NPs. Our group has already started working on the mixture of DES and IL as an efficient solvent mixture for the synthesis of N-doped carbon dots (CDs) for light harvesting applications.[180] A DES composed of choline-chloride and ethylene glycol was used to support the self-assembly of surface active choline oleate [Cho][Ole], which stabilized the CDs produced by gelatin as the carbon source.

There is still a lot to investigate at the smallest scale of dimensions tuned by reaction conditions for useful applications in the fields of chemical sciences that are both unknown and interesting at the same time. The need for more photocatalytic materials is important also because we need more recyclable and vast sources of energy as alternatives to conventional ones. Therefore, nanomaterials that are efficient in harvesting solar energy, visible light at best, can prove to be helpful in maintaining sustainable surroundings in catalytic reactions. This feature article paves the way for the synthesis of novel and environment-friendly molecules to provide a templating effect for efficient shape and size control of nanomaterials. The synthetic route employed for the NP formation also leaves an impact on their properties which drives the mass-scale application of nanotechnology in various fields of importance.

Data availability

No primary research results have been included and no new data were generated or analyzed as part of this review.

Conflicts of interest

There are no conflicts to declare.

Acknowledgements

We are grateful to UGC, India, for their UGC-CAS program and DST, India, for the FIST program awarded to the Department of Chemistry, Guru Nanak Dev University, Amritsar. K. S. is thankful to CSIR for the SPM fellowship. DST-SERB (CRG/2021/005897) and CSIR (01(3018)/21/EMR-II) are highly acknowledged for providing funds for this work. A special thanks to all the cited researchers who contributed to the work (Preet Shikha, B. S. Randhawa, Gurbir Singh, Komal Arora, Manvir Kaur, Manpreet Singh, Harjinder Singh, Karthikeyan Sekar, Bilal Ahmad Shiekh, Kuldeep Singh, Arvind Kumar).

Notes and references

1 G. A. Ozin, *Adv. Mater.*, 1992, **4**, 612–649.
2 P. Mulvaney, *ACS Nano*, 2015, **9**, 2215–2217.
3 A. Thiaville and J. Miltat, *Science*, 1999, **284**, 1939–1940.
4 S. Peiris, J. McMurtrie and H. Y. Zhu, *Catal. Sci. Technol.*, 2016, **6**, 320–338.
5 M. Shim and P. Guyot-Sionnest, *Nature*, 2000, **407**, 981–983.
6 A. P. Alivisatos, *J. Phys. Chem.*, 1996, **100**, 13226–13239.
7 K. Awazu, M. Fujimaki, C. Rockstuhl, J. Tominaga, H. Murakami, Y. Ohki, N. Yoshida and T. Watanabe, *J. Am. Chem. Soc.*, 2008, **130**, 1676–1680.
8 S. Cao, Y. Chen, C. J. Wang, P. He and W. F. Fu, *Chem. Commun.*, 2014, **50**, 10427.
9 P. Fageria, S. Gangopadhyay and S. Pande, *RSC Adv.*, 2014, **4**, 24962–24972.
10 N. Wiesmann, W. Tremel and J. Brieger, *J. Mater. Chem. B*, 2020, **8**, 4973–4989.
11 M. Cueto, M. Piedrahita, C. Caro, B. Martínez-Haya, M. Sanz, M. Oujja and M. Castillejo, *J. Phys. Chem. C*, 2014, **118**, 11432–11439.
12 S. Linic, P. Christopher and D. B. Ingram, *Nat. Mater.*, 2011, **10**, 911–921.
13 K. S. Novoselov, A. K. Geim, S. V. Morozov, D. Jiang, Y. Zhang, S. V. Dubonos, I. V. Grigorieva and A. A. Firsov, *Science*, 2004, **306**, 666–669.
14 M. Chhowalla, H. S. Shin, G. Eda, L. J. Li, K. P. Loh and H. Zhang, *Nat. Chem.*, 2013, **5**, 263–275.
15 Y. Du, Z. Yin, J. Zhu, X. Huang, X. J. Wu, Z. Zeng, Q. Yan and H. Zhang, *Nat. Commun.*, 2012, **3**, 1177.
16 J. N. Coleman, M. Lotya, A. O'Neill, S. D. Bergin, P. J. King, U. Khan, K. Young, A. Gaucher, S. De, R. J. Smith, I. V. Shvets, S. K. Arora, G. Stanton, H.-Y. Kim, K. Lee, G. T. Kim, G. S. Duesberg, T. Hallam, J. J. Boland, J. J. Wang, J. F. Donegan, J. C. Grunlan, G. Moriarty, A. Shmeliov, R. J. Nicholls, J. M. Perkins, E. M. Grieveson, K. Theuwissen, D. W. McComb, P. D. Nellist and V. Nicolosi, *Science*, 2011, **331**, 568–571.
17 V. Eswaraiah, Q. Zeng, Y. Long and Z. Liu, *Small*, 2016, **12**, 3480–3502.
18 Y. Lin, T. V. Williams and J. W. Connell, *J. Phys. Chem. Lett.*, 2010, **1**, 277–283.
19 Y. Peng, Y. Li, Y. Ban, H. Jin, W. Jiao, X. Liu and W. Yang, *Science*, 2014, **346**, 1356–1359.
20 M. Naguib, M. Kurtoglu, V. Presser, J. Lu, J. Niu, M. Heon, L. Hultman, Y. Gogotsi and M. W. Barsoum, *Adv. Mater.*, 2011, **23**, 4248–4253.
21 L. Rapoport, N. Fleischer and R. Tenne, *J. Mater. Chem.*, 2005, **15**, 1782.
22 W. Zhou, Z. Yin, Y. Du, X. Huang, Z. Zeng, Z. Fan, H. Liu, J. Wang and H. Zhang, *Small*, 2013, **9**, 140–147.
23 W. Ho, J. C. Yu, J. Lin, J. Yu and P. Li, *Langmuir*, 2004, **20**, 5865–5869.

24 F. Raza, D. Yim, J. H. Park, H. I. Kim, S. J. Jeon and J. H. Kim, *J. Am. Chem. Soc.*, 2017, **139**, 14767–14774.
25 B. Wiley, Y. Sun and Y. Xia, *Acc. Chem. Res.*, 2007, **40**, 1067–1076.
26 M. Maillard, P. Huang and L. Brus, *Nano Lett.*, 2003, **3**, 1611–1615.
27 M. Han, Q. Liu, J. He, Y. Song, Z. Xu and J. M. Zhu, *Adv. Mater.*, 2007, **19**, 1096–1100.
28 H. Zhang and H. Cui, *Langmuir*, 2009, **25**, 2604–2612.
29 J. Park, J. Joo, S. G. Kwon, Y. Jang and T. Hyeon, *Angew. Chem., Int. Ed.*, 2007, **46**, 4630–4660.
30 K. M. Koczkur, S. Mourdikoudis, L. Polavarapu and S. E. Skrabalak, *Dalton Trans.*, 2015, **44**, 17883–17905.
31 X. Xia, J. Zeng, L. K. Oetjen, Q. Li and Y. Xia, *J. Am. Chem. Soc.*, 2012, **134**, 1793–1801.
32 A. I. A. Abd El-Mageed, A. E. Shalan, L. A. Mohamed, H. A. Essawy, F. Taha and A. K. F. Dyab, *Polym. Eng. Sci.*, 2021, **61**, 234–244.
33 A. I. A. Abd El-Mageed, A. K. F. Dyab, L. A. Mohamed, F. Taha and H. A. Essawy, *Polym. Bull.*, 2022, **79**, 3379–3393.
34 Y. Sun and Y. Xia, *Adv. Mater.*, 2002, **14**, 833.
35 W. S. Hummers and R. E. Offeman, *J. Am. Chem. Soc.*, 1958, **80**, 1339.
36 V. Nicolosi, M. Chhowalla, M. G. Kanatzidis, M. S. Strano and J. N. Coleman, *Science*, 2013, **340**, 1226419.
37 G. Cunningham, M. Lotya, C. S. Cucinotta, S. Sanvito, S. D. Bergin, R. Menzel, M. S. P. Shaffer and J. N. Coleman, *ACS Nano*, 2012, **6**, 3468–3480.
38 P. T. Anastas and M. M. Kirchhoff, *Acc. Chem. Res.*, 2002, **35**, 686–694.
39 R. A. Sheldon, *Chem. Soc. Rev.*, 2012, **41**, 1437–1451.
40 A. M. El-Khawaga, A. Zidan and A. I. A. A. El-Mageed, *J. Mol. Struct.*, 2023, **1281**, 135148.
41 A. M. El-Khawaga, H. Tantawy, M. A. Elsayed and A. I. A. Abd El-Mageed, *Sci. Rep.*, 2022, **12**, 17075.
42 A. M. El-Khawaga, A. A. Farrag, M. A. Elsayed, G. S. El-Sayyad and A. I. El-Batal, *J. Cluster Sci.*, 2022, **33**, 197–213.
43 J.-C. Ni, Y.-X. Luan, X.-F. Wang, Z. Tan and X.-Z. Song, *J. Mater. Chem. A*, 2024, **12**, 14268–14301.
44 R. S. Varma, *ACS Sustainable Chem. Eng.*, 2016, **4**, 5866–5878.
45 J. E. Camp, J. J. Dunsford, E. P. Cannons, W. J. Restorick, A. Gadzhieva, M. W. Fay and R. J. Smith, *ACS Sustainable Chem. Eng.*, 2014, **2**, 500–505.
46 Z. M. Alvand, H. R. Rajabi, A. Mirzaei and F. Sajadiasl, *Surf. Interfaces*, 2021, **25**, 101182.
47 K. Shivaji, S. Mani, P. Ponmurugan, C. S. De Castro, M. Lloyd Davies, M. G. Balasubramanian and S. Pitchaimuthu, *ACS Appl. Nano Mater.*, 2018, **1**, 1683–1693.
48 in *Ionic Liquids in Synthesis*, ed. P. Wasserscheid and T. Welton, Wiley, 1st edn, 2007.
49 M. Smiglak, J. M. Pringle, X. Lu, L. Han, S. Zhang, H. Gao, D. R. MacFarlane and R. D. Rogers, *Chem. Commun.*, 2014, **50**, 9228–9250.
50 T. Welton, *Chem. Rev.*, 1999, **99**, 2071–2084.
51 Y. Liu, P. G. Jessop, M. Cunningham, C. A. Eckert and C. L. Liotta, *Science*, 2006, **313**, 958–960.
52 D. R. MacFarlane, M. Forsyth, P. C. Howlett, J. M. Pringle, J. Sun, G. Annat, W. Neil and E. I. Izgorodina, *Acc. Chem. Res.*, 2007, **40**, 1165–1173.
53 S. P. M. Ventura, F. A. E. Silva, M. V. Quental, D. Mondal, M. G. Freire and J. A. P. Coutinho, *Chem. Rev.*, 2017, **117**, 6984–7052.
54 F. J. M. Rutten, H. Tadesse and P. Licence, *Angew. Chem., Int. Ed.*, 2007, **46**, 4163–4165.
55 S. Hisamitsu, N. Yanai and N. Kimizuka, *Angew. Chem.*, 2015, **127**, 11712–11716.
56 M. Antonietti, D. Kuang, B. Smarsly and Y. Zhou, *Angew. Chem., Int. Ed.*, 2004, **43**, 4988–4992.
57 H. F. Gaiser, R. Popescu, D. Gerthsen and C. Feldmann, *Chem. Commun.*, 2020, **56**, 2312–2315.
58 J. Hildebrandt, A. Taubert and A. F. Thünemann, *ChemistryOpen*, 2024, **13**, e202300106.
59 A. Schmitz, H. Meyer, M. Meischein, A. G. Manjón, L. Schmolke, B. Giesen, C. Schlüsener, P. Simon, Y. Grin, R. A. Fischer, C. Scheu, A. Ludwig and C. Janiak, *RSC Adv.*, 2020, **10**, 12891–12899.
60 S. S. Mali, C. A. Betty, P. N. Bhosale, R. S. Devan, Y.-R. Ma, S. S. Kolekar and P. S. Patil, *CrystEngComm*, 2012, **14**, 1920.
61 Z. L. Xie, X. Huang, M. M. Titirici and A. Taubert, *RSC Adv.*, 2014, **4**, 37423–37430.
62 E. Ahmed and M. Ruck, *Angew. Chem., Int. Ed.*, 2012, **51**, 308–309.
63 W. J. Ji, Q. G. Zhai, S. N. Li, Y. C. Jiang and M. C. Hu, *Chem. Commun.*, 2011, **47**, 3834.
64 O. Russina, F. Lo Celso, N. V. Plechkova and A. Triolo, *J. Phys. Chem. Lett.*, 2017, **8**, 1197–1204.
65 J. N. A. C. Lopes and A. A. H. Pádua, *J. Phys. Chem. B*, 2006, **110**, 3330–3335.
66 T. Burankova, J. F. M. Cardozo, D. Rauber, A. Wildes and J. P. Embs, *Sci. Rep.*, 2018, **8**, 16400.
67 K. Bernardino, *ACS Nano*, 2024, **18**, 20389–20400.
68 J. Bowers, C. P. Butts, P. J. Martin, M. C. Vergara-Gutierrez and R. K. Heenan, *Langmuir*, 2004, **20**, 2191–2198.
69 J. Wang, H. Wang, S. Zhang, H. Zhang and Y. Zhao, *J. Phys. Chem. B*, 2007, **111**, 6181–6188.
70 H. Wang, J. Wang, S. Zhang and X. Xuan, *J. Phys. Chem. B*, 2008, **112**, 16682–16689.
71 T. J. Trivedi, K. S. Rao, T. Singh, S. K. Mandal, N. Sutradhar, A. B. Panda and A. Kumar, *ChemSusChem*, 2011, **4**, 604–608.
72 K. S. Rao, P. S. Gehlot, T. J. Trivedi and A. Kumar, *J. Colloid Interface Sci.*, 2014, **428**, 267–275.
73 P. S. Gehlot, A. Kulshrestha, P. Bharmoria, K. Damarla, K. Chokshi and A. Kumar, *ACS Omega*, 2017, **2**, 7451–7460.
74 C. S. Buettner, A. Cognigni, C. Schröder and K. Bica-Schröder, *J. Mol. Liq.*, 2022, **347**, 118160.
75 M. Blesic, M. Swadźba-Kwaśny, J. D. Holbrey, J. N. C. Lopes, K. R. Seddon and L. P. N. Rebelo, *Phys. Chem. Chem. Phys.*, 2009, **11**, 4260.
76 in *Applications of Ionic Liquids in Science and Technology*, ed. S. Handy, IntechOpen, 2011.
77 Z. Huang, J. Gong and Z. Nie, *Acc. Chem. Res.*, 2019, **52**, 1125–1133.
78 Y. Zhao, G. Cui, J. Wang and M. Fan, *Inorg. Chem.*, 2009, **48**, 10435–10441.
79 K. S. Rao, T. J. Trivedi and A. Kumar, *J. Phys. Chem. B*, 2012, **116**, 14363–14374.
80 Y. Sun, B. T. Mayers and Y. Xia, *Nano Lett.*, 2002, **2**, 481–485.
81 T. Nakashima and N. Kimizuka, *J. Am. Chem. Soc.*, 2003, **125**, 6386–6387.
82 X. Liu, J. Ma, P. Peng and W. Zheng, *Langmuir*, 2010, **26**, 9968–9973.
83 X. Yuan, N. Yan, C. Xiao, C. Li, Z. Fei, Z. Cai, Y. Kou and P. J. Dyson, *Green Chem.*, 2010, **12**, 228.
84 C. W. Scheeren, G. Machado, S. R. Teixeira, J. Morais, J. B. Domingos and J. Dupont, *J. Phys. Chem. B*, 2006, **110**, 13011–13020.
85 D. Zhang, T. Okajima, D. Lu and T. Ohsaka, *Langmuir*, 2013, **29**, 11931–11940.
86 Y. Yu, T. Hu, X. Chen, K. Xu, J. Zhang and J. Huang, *Chem. Commun.*, 2011, **47**, 3592.
87 Y. Hatakeyama, K. Asakura, S. Takahashi, K. Judai and K. Nishikawa, *J. Phys. Chem. C*, 2014, **118**, 27973–27980.
88 M. Meischein, A. Garzón-Manjón, T. Frohn, H. Meyer, S. Salomon, C. Scheu and A. Ludwig, *ACS Comb. Sci.*, 2019, **21**, 743–752.
89 T. Soejima and N. Kimizuka, *Chem. Lett.*, 2005, **34**, 1234–1235.
90 R. Bussamara, W. W. M. Melo, J. D. Scholten, P. Migowski, G. Marin, M. J. M. Zapata, G. Machado, S. R. Teixeira, M. A. Novak and J. Dupont, *Dalton Trans.*, 2013, **42**, 14473.
91 T. Alammar, H. Noei, Y. Wang, W. Grünert and A. V. Mudring, *ACS Sustainable Chem. Eng.*, 2015, **3**, 42–54.
92 Z. Lou, B. Huang, X. Qin, X. Zhang, Z. Wang, Z. Zheng, H. Cheng, P. Wang and Y. Dai, *CrystEngComm*, 2011, **13**, 1789.
93 A. Podgoršek, A. S. Pensado, C. C. Santini, M. F. C. Gomes and A. A. H. Pádua, *J. Phys. Chem. C*, 2013, **117**, 3537–3547.
94 A. Imanishi, *Chem. Rec.*, 2023, **23**, e202300110.
95 R. L. White, *J. Appl. Phys.*, 1969, **40**, 1061–1069.
96 S. Li, L. Jing, W. Fu, L. Yang, B. Xin and H. Fu, *Mater. Res. Bull.*, 2007, **42**, 203–212.
97 K. Li, D. Wang, F. Wu, T. Xie and T. Li, *Mater. Chem. Phys.*, 2000, **64**, 269–272.
98 S. Royer, F. Bérubé and S. Kaliaguine, *Appl. Catal., A*, 2005, **282**, 273–284.
99 J. Leng, S. Li, Z. Wang, Y. Xue and D. Xu, *Mater. Lett.*, 2010, **64**, 1912–1914.
100 S. Thirumalairajan, K. Girija, V. Ganesh, D. Mangalaraj, C. Viswanathan and N. Ponpandian, *Cryst. Growth Des.*, 2013, **13**, 291–302.
101 K. M. Parida, K. H. Reddy, S. Martha, D. P. Das and N. Biswal, *Int. J. Hydrogen Energy*, 2010, **35**, 12161–12168.

102 B. Ita, P. Murugavel, V. Ponnambalam and A. R. Raju, *J. Chem. Sci.*, 2003, **115**, 519–524.
103 R. Hu, C. Li, X. Wang, Y. Sun, H. Jia, H. Su and Y. Zhang, *Catal. Commun.*, 2012, **29**, 35–39.
104 L. Hou, G. Sun, K. Liu, Y. Li and F. Gao, *J. Sol–Gel Sci. Technol.*, 2006, **40**, 9–14.
105 R. Pushpa, D. Daniel and D. P. Butt, *Solid State Ionics*, 2013, **249–250**, 184–190.
106 M. V. Kuznetsov, Q. A. Pankhurst, I. P. Parkin and Y. G. Morozov, *J. Mater. Chem.*, 2001, **11**, 854–858.
107 H. Wu, R. Hu, T. Zhou, C. Li, W. Meng and J. Yang, *CrystEngComm*, 2015, **17**, 3859–3865.
108 P. Shikha, T. S. Kang and B. S. Randhawa, *RSC Adv.*, 2015, **5**, 96799–96808.
109 O. A. El Seoud, P. A. R. Pires, T. Abdel-Moghny and E. L. Bastos, *J. Colloid Interface Sci.*, 2007, **313**, 296–304.
110 P. Shikha, Komal, T. S. Kang and B. S. Randhawa, *J. Alloys Compd.*, 2017, **701**, 788–796.
111 A. K. Azad, A. Mellergård, S.-G. Eriksson, S. A. Ivanov, S. M. Yunus, F. Lindberg, G. Svensson and R. Mathieu, *Mater. Res. Bull.*, 2005, **40**, 1633–1644.
112 K. Arora, P. Shikha, R. M. K. Abdelbaky and T. S. Kang, *Appl. Phys. A: Mater. Sci. Process.*, 2021, **127**, 141.
113 M. B. Gawande, P. S. Branco and R. S. Varma, *Chem. Soc. Rev.*, 2013, **42**, 3371.
114 D. Cantillo, M. Baghbanzadeh and C. O. Kappe, *Angew. Chem., Int. Ed.*, 2012, **51**, 10190–10193.
115 R. Hudson, Y. Feng, R. S. Varma and A. Moores, *Green Chem.*, 2014, **16**, 4493–4505.
116 R. M. Cornell and U. Schwertmann, *The Iron Oxides: Structure, Properties, Reactions, Occurences and Uses*, Wiley, 1st edn, 2003.
117 L. Liu, H. Z. Kou, W. Mo, H. Liu and Y. Wang, *J. Phys. Chem. B*, 2006, **110**, 15218–15223.
118 S. B. Wang, Y. L. Min and S. H. Yu, *J. Phys. Chem. C*, 2007, **111**, 3551–3554.
119 C. Y. Cao, J. Qu, W. S. Yan, J. F. Zhu, Z. Y. Wu and W. G. Song, *Langmuir*, 2012, **28**, 4573–4579.
120 X. C. Jiang, A. B. Yu, W. R. Yang, Y. Ding, C. X. Xu and S. Lam, *J. Nanopart. Res.*, 2010, **12**, 877–893.
121 F. Bødker, M. F. Hansen, C. B. Koch, K. Lefmann and S. Mørup, *Phys. Rev. B: Condens. Matter Mater. Phys.*, 2000, **61**, 6826–6838.
122 M. Khalil, J. Yu, N. Liu and R. L. Lee, *J. Nanopart. Res.*, 2014, **16**, 2362.
123 M. Zhu, Y. Wang, D. Meng, X. Qin and G. Diao, *J. Phys. Chem. C*, 2012, **116**, 16276–16285.
124 J. Lian, X. Duan, J. Ma, P. Peng, T. Kim and W. Zheng, *ACS Nano*, 2009, **3**, 3749–3761.
125 M. Behboudnia, A. Habibi-Yangjeh, Y. Jafari-Tarzanag and A. Khodayari, *J. Cryst. Growth*, 2008, **310**, 4544–4548.
126 M. Leskiv, C. E. S. Bernardes, M. E. M. Da Piedade and J. N. C. Lopes, *J. Phys. Chem. B*, 2010, **114**, 13179–13188.
127 Q. G. Zhang, N. N. Wang and Z. W. Yu, *J. Phys. Chem. B*, 2010, **114**, 4747–4754.
128 C. E. S. Bernardes, M. E. M. Da Piedade and J. N. C. Lopes, *J. Phys. Chem. B*, 2011, **115**, 2067–2074.
129 P. Shikha, B. S. Randhawa and T. S. Kang, *RSC Adv.*, 2015, **5**, 51158–51168.
130 Y. P. He, Y. M. Miao, C. R. Li, S. Q. Wang, L. Cao, S. S. Xie, G. Z. Yang, B. S. Zou and C. Burda, *Phys. Rev. B: Condens. Matter Mater. Phys.*, 2005, **71**, 125411.
131 T. Takagahara and K. Takeda, *Phys. Rev. B: Condens. Matter Mater. Phys.*, 1992, **46**, 15578–15581.
132 A. Taubert, *Angew. Chem., Int. Ed.*, 2004, **43**, 5380–5382.
133 K. Komal, H. Kaur, M. Kainth, S. S. Meena and T. S. Kang, *RSC Adv.*, 2019, **9**, 41803–41810.
134 L. Xu, J. Xia, K. Wang, L. Wang, H. Li, H. Xu, L. Huang and M. He, *Dalton Trans.*, 2013, **42**, 6468.
135 L. Xu, J. Xia, L. Wang, J. Qian, H. Li, K. Wang, K. Sun and M. He, *Chem. – Eur. J.*, 2014, **20**, 2244–2253.
136 P. Roy, A. P. Periasamy, C. Chuang, Y. R. Liou, Y. F. Chen, J. Joly, C. T. Liang and H. T. Chang, *New J. Chem.*, 2014, **38**, 4946–4951.
137 K. Komal, P. Shikha and T. S. Kang, *New J. Chem.*, 2017, **41**, 7407–7416.
138 S. Sarina, E. R. Waclawik and H. Zhu, *Green Chem.*, 2013, **15**, 1814.
139 K. M. Metz, S. E. Sanders, J. P. Pender, M. R. Dix, D. T. Hinds, S. J. Quinn, A. D. Ward, P. Duffy, R. J. Cullen and P. E. Colavita, *ACS Sustainable Chem. Eng.*, 2015, **3**, 1610–1617.
140 Z. Bian, T. Tachikawa, P. Zhang, M. Fujitsuka and T. Majima, *J. Am. Chem. Soc.*, 2014, **136**, 458–465.
141 L. Kuai, B. Geng, X. Chen, Y. Zhao and Y. Luo, *Langmuir*, 2010, **26**, 18723–18727.
142 P. Wang, B. Huang, X. Qin, X. Zhang, Y. Dai, J. Wei and M. Whangbo, *Angew. Chem., Int. Ed.*, 2008, **47**, 7931–7933.
143 S. Ghosh, A. Saraswathi, S. S. Indi, S. L. Hoti and H. N. Vasan, *Langmuir*, 2012, **28**, 8550–8561.
144 G. Loget, T. C. Lee, R. W. Taylor, S. Mahajan, O. Nicoletti, S. T. Jones, R. J. Coulston, V. Lapeyre, P. Garrigue, P. A. Midgley, O. A. Scherman, J. J. Baumberg and A. Kuhn, *Small*, 2012, **8**, 2698–2703.
145 A. E. Kossak, B. O. Stephens, Y. Tian, P. Liu, M. Chen and T. J. Kempa, *Nano Lett.*, 2018, **18**, 2324–2328.
146 G. Singh, K. Komal, G. Singh, M. Kaur and T. S. Kang, *J. Mater. Chem. A*, 2019, **7**, 5185–5189.
147 G. Singh, R. Kamoj, V. Singh Mithu, V. Chauhan, T. Kaur, G. Kaur, S. Singh and T. Singh Kang, *J. Colloid Interface Sci.*, 2017, **496**, 278–289.
148 R. Takahashi, M. Fujishima, H. Tada and T. Soejima, *ChemNanoMat*, 2020, **6**, 1485–1495.
149 R. Purbia and S. Paria, *Dalton Trans.*, 2017, **46**, 890–898.
150 K. Sharma, H. Singh, G. Singh, N. Kaur, P. Kumar Pati, K. Singh, A. Kumar and T. S. Kang, *Nanoscale*, 2024, **16**, 17549–17558.
151 M. Zhu, P. Chen and M. Liu, *Langmuir*, 2012, **28**, 3385–3390.
152 A. Goswami, R. G. Kadam, J. Tuček, Z. Sofer, D. Bouša, R. S. Varma, M. B. Gawande and R. Zbořil, *Chem. Eng. J.*, 2020, **382**, 122469.
153 A. Goswami, A. K. Rathi, C. Aparicio, O. Tomanec, M. Petr, R. Pocklanova, M. B. Gawande, R. S. Varma and R. Zboril, *ACS Appl. Mater. Interfaces*, 2017, **9**, 2815–2824.
154 S. Bai, J. Ge, L. Wang, M. Gong, M. Deng, Q. Kong, L. Song, J. Jiang, Q. Zhang, Y. Luo, Y. Xie and Y. Xiong, *Adv. Mater.*, 2014, **26**, 5689–5695.
155 A. Du, Y. H. Ng, N. J. Bell, Z. Zhu, R. Amal and S. C. Smith, *J. Phys. Chem. Lett.*, 2011, **2**, 894–899.
156 K. Arora, S. Karthikeyan, B. A. Shiekh, M. Kaur, H. Singh, G. R. Bhadu and T. S. Kang, *New J. Chem.*, 2020, **44**, 15567–15573.
157 K. Arora, G. Singh, S. Karthikeyan and T. S. Kang, *Nanoscale Adv.*, 2020, **2**, 4770–4776.
158 K. Arora, M. Kaur, H. Singh, S. Karthikeyan and T. S. Kang, *Appl. Surf. Sci.*, 2021, **553**, 149555.
159 X. Hong, J. Liu, B. Zheng, X. Huang, X. Zhang, C. Tan, J. Chen, Z. Fan and H. Zhang, *Adv. Mater.*, 2014, **26**, 6250–6254.
160 D. Sarkar, X. Xie, J. Kang, H. Zhang, W. Liu, J. Navarrete, M. Moskovits and K. Banerjee, *Nano Lett.*, 2015, **15**, 2852–2862.
161 H. Singh, K. Sharma, K. Sekar, M. Singh and T. S. Kang, *Surf. Interfaces*, 2024, **48**, 104272.
162 T. Soejima, H. Inoue, K. Egashira, Y. Yan and H. Tada, *Chem. Commun.*, 2023, **59**, 1449–1452.
163 H. Inoue, S. Naya, A. Akita, H. Sugime and H. Tada, *Chem. – Eur. J.*, 2022, **28**, e202201653.
164 S. Luo, X. Ren, H. Lin, H. Song and J. Ye, *Chem. Sci.*, 2021, **12**, 5701–5719.
165 X. Zhu, Y. Lin, J. San Martin, Y. Sun, D. Zhu and Y. Yan, *Nat. Commun.*, 2019, **10**, 2843.
166 C. Rosso, G. Filippini, A. Criado, M. Melchionna, P. Fornasiero and M. Prato, *ACS Nano*, 2021, **15**, 3621–3630.
167 A. Kumar, P. Choudhary, A. Kumar, P. H. C. Camargo and V. Krishnan, *Small*, 2022, **18**, 2101638.
168 S. C. Abeyweera, K. D. Rasamani and Y. Sun, *Acc. Chem. Res.*, 2017, **50**, 1754–1761.
169 Z. Li and Y. Sun, *J. Mater. Chem. A*, 2013, **1**, 6786.
170 Z. Li, J. S. Okasinski, D. J. Gosztola, Y. Ren and Y. Sun, *J. Mater. Chem. C*, 2015, **3**, 58–65.
171 B. Cai, J. Wang, D. Han, S. Gan, Q. Zhang, Z. Wu and L. Niu, *Nanoscale*, 2013, **5**, 10989.
172 C. An, J. Wang, C. Qin, W. Jiang, S. Wang, Y. Li and Q. Zhang, *J. Mater. Chem.*, 2012, **22**, 13153.
173 H. Jia, Y. Dou, Y. Yang, F. Li and C. Zhang, *Nanoscale*, 2021, **13**, 20289–20298.
174 M. Zhu, C. Chen, P. Chen, B. Lei, W. Ma and M. Liu, *Phys. Chem. Chem. Phys.*, 2013, **15**, 12709.

175 M. Kaur, G. Singh, K. Damarla, G. Singh, H. Wang, J. Wang, V. K. Aswal, A. Kumar and T. S. Kang, *Phys. Chem. Chem. Phys.*, 2020, **22**, 169–178.
176 A. P. Abbott, G. Capper, D. L. Davies, R. K. Rasheed and V. Tambyrajah, *Chem. Commun.*, 2003, 70–71.
177 E. L. Smith, A. P. Abbott and K. S. Ryder, *Chem. Rev.*, 2014, **114**, 11060–11082.
178 H. Kaur, M. Singh, H. Singh, M. Kaur, G. Singh, K. Sekar and T. S. Kang, *Green Chem.*, 2022, **24**, 2953–2961.
179 H. Kaur, M. Singh, K. Singh, A. Kumar and T. S. Kang, *Green Chem.*, 2023, **25**, 5172–5181.
180 K. Damarla, S. Mehra, T. S. Kang, S. Yadav, A. Mishra and A. Kumar, *Mater. Adv.*, 2020, **1**, 3476–3482.

